ABSTRACT

KULKARNI, NILAY ATUL. Methodology Development for High-To-Low Information of Subchannel Code CTF with CFD Code Nek5000. (Under the direction of Dr. Maria Avramova).

Precise thermal hydraulic analysis of reactor core is essential for safety and power analysis of a nuclear reactor. Complete reactor core calculations can be carried out using subchannel codes, but these codes often lack the resolution and fidelity to capture physical phenomenon occurring at smaller scales. Computational Fluid Dynamics (CFD) on the other hand can capture these phenomena but it is computationally expensive.

The High-To-Low (Hi2Lo) model fidelity information seeks to bridge this gap by using data extracted from high-fidelity modeling and simulation (M&S) tools such as CFD codes and applying it as informing parameters to improve macroscopic physical phenomenon M&S in CTF. In this study, a methodology is developed to inform the subchannel code CTF with the spectral element code Nek5000. Subchannels are modeled with various spacer grids addressed in the PSBT benchmark and turbulent simulation are carried out using Large Eddy Simulation (LES) turbulence modelling. With these simulations the grid loss coefficient and the custom friction factor are calibrated to be informed to account for form and friction pressure loss in CTF. Friction factor calibration is carried out using friction velocity data obtained from different levels of mesh refinement over a range of flowrates and different levels of mesh refinement. With the friction factor calibration, an attempt is made to demonstrate the propagation of mesh-based uncertainty from high-fidelity Nek5000 to lower fidelity CTF.

The presence of spacer grids not only causes form pressure loss but also causes augmentation in the turbulence locally which causes mixing between adjacent subchannels and affects the heat transfer from the fuel rods surface to the coolant. In this study, a center-center subchannel

configuration with the simplified spacer grids is modeled to extract Hi2Lo data for a single-phase turbulent mixing multiplier and to calculate the enhanced heat transfer coefficient.

Methodology Development for High-To-Low Information of Subchannel Code CTF with CFD Code Nek5000

by
Nilay Atul Kulkarni

A thesis submitted to the Graduate Faculty of
North Carolina State University
in partial fulfillment of the
requirements for the degree of
Master of Science

Nuclear Engineering

Raleigh, North Carolina
2023

APPROVED BY:

_____	_____
Dr. Maria Avramova Committee Chair	Dr. Kostadin Ivanov
_____	
Dr. David Holler	

DEDICATION

To my parents and my wife for all the love and support

BIOGRAPHY

Nilay Atul Kulkarni was born on April 8th, 1996, to Mr. Atul Kulkarni and Mrs. Nilakshi Kulkarni in Akola, Maharashtra, India. After completing his high school education, Nilay pursued a bachelor's degree in Mechanical Engineering at Manipal Institute of Technology, Manipal, India and graduated in 2017 with distinction. After completing his bachelor's degree, he moved to Raleigh in 2017 to pursue his master's in Mechanical Engineering at North Carolina State University. He received his master's degree in the 2019 Fall term and under the guidance of Dr. C. Kleinstreuer in the Computational Multi-Physics Lab at NC State. After this he joined the Nuclear Engineering department where he will be receiving another master's degree in Fall 2022.

ACKNOWLEDGMENTS

I want to take this opportunity to thank Dr. Maria Avramova for giving me the opportunity to pursue my subject of interest and for her guidance and patience with me. I also want to thank Dr. David Holler for his support and his direction throughout the duration of my studies.

This thesis wouldn't have been possible if not for the unconditional support from my parents. They always believed in me and talking me through times when I needed their emotional support. Seriously, I can't thank them enough for that.

A special paragraph for my wife Chaitee, who has been with me in-person through the whirl wind of emotion that has been the past two years. I can't thank her enough for keeping me sane through it and for being my rock through the tough times while being a graduate student herself. I am truly grateful for having her in my life.

Special thanks to Dr. Marc-Olivier Delchini for his mentorship and his advice and all the help right from setting up simulations to trouble shooting them with me. I also want to thank him for his patience with me and motivating me to be a good researcher. I also want to thank Joseph Fustero for all the help he's given me throughout my time in working on this project.

This work is supported by the US Department of Energy Nuclear Energy University Programs (NEUP) Project 18-15104 (DE-NE0008754) and has made use of the resources of the High-Performance Computing Center at Idaho National Laboratory, which is supported by the Office of Nuclear Energy of the US Department of Energy and the Nuclear Science User Facilities under Contract No. DE-AC07-05ID14517. The authors would like to thank Dr. Dillon Shaver from Argonne National Laboratory for kindly providing the Fortran subroutine to compute the surface average using the thin-volume approach. This research also used resources of the Compute and Data Environment for Science (CADES) at the Oak Ridge National Laboratory,

which is supported by the Office of Science of the U.S. Department of Energy under Contract No. DE-AC05-00OR22725.

TABLE OF CONTENTS

LIST OF TABLES

LIST OF FIGURES

CHAPTER 1: INTRODUCTION

The nuclear reactor is one of the most sophisticated engineering implementations in the past century which allows us to harness fission energy to generate heat and ultimately electricity. There are multitudes of physical phenomena occurring inside the nuclear reactor which are not only simultaneous but also coupled with one another. One of these domains is thermal hydraulics (TH) which deals with study of flows, turbulence, mixing and heat transfer from the fissionable or fissile material to the coolant. Experimental analysis of a nuclear reactor is very difficult not only from a safety point of view but also from an economical point of view. Thus, we rely on computational methods to simulate reactor conditions for analysis.

In general, there are three broad computational means to simulate TH behavior of a nuclear reactor. The first method is by using system codes. System codes use momentum, energy, and conservation equations but on a coarse grid. Some codes use a set of one-dimensional (1D) balance equations for tracking primary dependent variables such as pressure, void fraction, liquid and vapor phase velocities and their respective energy balances and boron transport. Closure relations are used to provide variables that cannot be directly calculated at a certain level of fidelity. The code includes many generic component models from which general systems can be simulated. The component models include pumps, valves, pipes, heat releasing or absorbing structures, electric heaters, jet pumps, turbines, separators, accumulators, and control system components.

The second approach is the subchannel analysis. In this method each subchannel is represented as a separate control volume, which can be divided into multiple axial sections. The subchannel control volume represents the space available for the coolant to flow surrounded by solid geometry. An example is that of a typical interior subchannel, where the flow space is

surrounded by three or four fuel rods. The spatial discretization in subchannel codes can be much finer compared to system codes over which conversation equations are solved. Subchannel codes also solve for the mass, momentum and energy equations but can vary depending on the treatment of the two-phase flow. These codes also require closure models to account for the macroscopic phenomenon such as pressure drop, coolant mixing, turbulent heat transfer. Due to such capabilities, subchannels codes allow modelling of complete fuel assemblies or even full core at relatively lower computationally cost and have better physical insight compared to the 1D codes. For example, in a system code where we can estimate the total heat output, subchannel codes can pin-point the location of hot-spots in an array of fuel assemblies.

Finally, Computational Fluid Dynamics (CFD) codes, which require a very fine spatial discretization compared to subchannel codes and can contain over a million elements per subchannel depending on the methodology implemented for the analysis. CFD solves for the same conservation equations without the need for approximations since its spatial resolution allows capturing of physical phenomena which occur at smallest scales. For example, the mesh surrounding a solid boundary needs to be fine enough in order to capture the viscous near wall effects, or the mesh in the bulk fluid needs to be fine enough to capture the eddies that are generated in turbulent flow. The major advantage of CFD is the ability to model flow around the smallest components of the reactor core. Depending on the implementation, CFD can provide flow details for turbulent eddied generated due to solid structures such as spacer grids.

Three main numerical approaches exist in TH codes, namely Finite Difference Method (FDM), Finite Volume Method (FVM) and Finite Element Method (FEM). FDM discretization is based upon the differential form of the partial differential equations (PDE) to be solved. Each derivative is replaced with an approximate difference formula. The computational domain is

usually divided into hexahedral cells (the grid), and the solution will be obtained at each nodal point. The FDM is easiest to understand when the physical grid is Cartesian, but through the use of curvilinear transforms the method can be extended to domains that are not easily represented by brick-shaped elements. The discretization results in a system of equation of the variable at nodal points, and once a solution is found, then we have a discrete representation of the solution. The FVM discretization is based on integral form of the PDEs to be solved i.e., the PDE is written in a form which can be solved for a given control volume. This involves solving of in-flux and out-flux of the variables within a mesh element. The basic advantage of this method over FDM is that it does not require the use of structured grids, and the effort to convert the given mesh in to structured numerical grid internally is completely avoided. The FEM discretization is based upon a piecewise representation of the solution in terms of specified basis functions. The computational domain is divided up into smaller domains (finite elements) and the solution in each element is constructed from the basis functions. The actual equations that are solved are typically obtained by restating the conservation equation in weak form: the field variables are written in terms of the basis functions, the equation is multiplied by appropriate test functions, and then integrated over an element. In summary, FVM and FDM provide a discrete solution whereas FEM provides a continuous solution. The accuracy of the different methods depends vastly on the type of problem and the spatial and temporal discretization, and the choice of basis functions in case of FEM. Opinions differ on the best method to use and CFD codes can be found using the different methods which have a reasonable level of accuracy.

The reactor vessel contains a large array of fuel assemblies. These fuel rods are held in place with mechanical structures called as spacer grids. The primary function of spacer grids is to maintain the rod pitch in fuel assemblies as well as to hold them steady and reduce vibration of

fuel due the high temperatures and high flowrates. The presence of these structures generates even more turbulence locally which is responsible for mixing of flow between neighboring subchannels. This mixing is a desirable phenomenon which leads to better heat transfer from the rods. Over time many different designs of spacer grids have been produced and utilized for assembling fuel rods. One of these spacer grids are designed with mixing vanes. The mixing vanes are an extrusion of the sheet metal used for the main body which is bent at an angle which directs the flow in a specific direction. From the CFD perspective, the spacer grids are geometrically complex structures which make the turbulent flow even more complicated as fluid passes over them. This obstruction to the flow also results in mixing between adjacent subchannels. Spacer grids are responsible for a local mixing phenomenon which aids in heat transfer from the fuel rods to the coolant. Moreover, due to the blockage provided to the flow, there is a pressure drop over the spacer grids. One more effect of this obstruction to flow is the pressure drop across spacer grids. Due to blockage to the total flow area in the subchannel, there is a pressure drop due to form loss that must be accounted for. Pressure drop modelling is very important as reduction in pressure will affect the thermo-physical properties of liquid. For example, and over prediction in the pressure drop will lead to lower pressure downstream, which in turn can cause incorrect prediction of bubble-formation. In CFD, the equations are solved on a finer scale and there is no need for closure equation or correlations to model the pressure drop. The effects of a solid obstruction and skin friction are reflected in the flow due to the high-resolution of the solution. Subchannel codes do not have such high resolution and therefore need correlations to model such terms and these correlations are usually experimentally determined.

1.1 Informing Low-Fidelity Codes using High-Fidelity Codes (Hi2Lo)

Lower fidelity modeling and simulation (M&S) codes, even though they solve the same mass momentum and energy equations, need closure terms to model for their prediction. These closure terms are usually provided as correlations which have been historically obtained from experimental data. To accommodate the physical phenomenon due to spacer grids, certain coefficients are applied which calculate the mass, momentum, and energy transfer from one subchannel to another. However, this limits the correlations to very specific test conditions and setups. Thus, application of such correlations outside the range of applicability can lead to erroneous prediction of the physical phenomenon. On the other hand, higher fidelity codes can resolve the turbulent flow in sufficient detail to quantify the phenomenon caused by spacer grids and can provide intricate details for the tiniest turbulent eddies in the viscous sub-layer (subject to refinement and models used). However, the major downside to the CFD codes is their high computation cost which limits the simulation scope of CFD to relatively small space domains (single subchannel or sub-assembly). Due to their complexity, the high-fidelity codes are computationally expensive, and may take on the order of hours to days to complete a simulation run. Lower fidelity codes take only a small fraction of the wall-time and computing resources and can simulate a much larger domain. This is where the concept of Hi2Lo comes in. Hi2Lo (High fidelity to Low fidelity model information) is the concept of using high-fidelity data from experiments and/or simulations to calibrate a low-fidelity code to return results consistent with the high-fidelity data. Since low-fidelity codes use correlations that are obtained from experimental data, these coefficients can be applied to all types of studies. CFD codes can be used to generate higher resolution data which captures all the physical phenomena. This data then can be post-processed to extract closure terms and coefficients that can be applied to

subchannel codes. A big advantage of this method is the reduction in computation cost by using subchannel codes. Also, due to the CFD augmented coefficients, the prediction capabilities are more accurate.

1.2 Motivation

In this work, the major motivation is applying concept of Hi2Lo for informing the subchannel code CTF with Nek5000. CTF is an advanced subchannel code that has been extensively validated for light water reactor applications. Nek5000 will be used for high fidelity simulations because it is a representative of CFD tools with high resolution with a numerical implementation which ensures higher order of accuracy of solution. CTF utilizes certain preset correlations to obtain wall friction coefficient as well as heat transfer coefficients. In this study, bare subchannel simulations were performed for a range on Reynolds numbers under isothermal conditions. This friction velocity calculated from Nek5000 is used to calibrate the custom friction factor available in CTF. This Hi2Lo off-line coupling will also be used to inform CTF of specific spacer grids effects such as enhanced heat transfer, turbulent mixing coefficient and grid loss coefficients for accurate form pressure loss predictions.

1.3 Objectives

For the Hi2Lo information of CTF, the CFD code Nek5000 will be applied. Due its spectral element method implementation, Nek5000 is known to have higher order of accuracy. CTF is an advanced subchannel code which uses empirical and experimentally obtained correlations to predict physical phenomena occurring in the reactor core. For the Hi2Lo setup, high-fidelity and high-resolution simulation will be conducted with Large Eddy Simulations (LES) turbulence modelling. Previous studies ((1)(2) (3)) in this domain have applied RANS k-epsilon turbulence model to extract relevant data from the CFD solution. In this study the LES,

which will be truly transient, sufficiently resolve turbulent eddies. These simulations will be time-averaged to extract the necessary parameters used for Hi2Lo information. Novel meshing methodology is applied to ensure accurate capturing for the turbulent flow by generating boundary layers for the complete spacer grid components and not only on the fuel rod surfaces. This will ensure that the y+<1 criterion is maintained at all solid walls encountered by the flow. Nek5000 simulations are carried to calibrate the custom friction factor available in CTF. There are correlations in literature that have been developed for simpler geometry, while in this study the friction correlation will be calibrated specifically for subchannel geometry. Lastly, the effects of simplified spacer grids will be accounted for turbulent mixing and enhanced heat transfer between a center-center subchannel configuration. The turbulent mixing coefficient will be measured across the gap region connecting the two subchannels. The enhanced heat transfer coefficient will be determined by extracting wall and bulk temperatures along the length of the subchannel.

CHAPTER 2: LITERATURE REVIEW

CFD has been widely applied in nuclear engineering applications. In this chapter, previous studies applying CFD to study the effects of spacer grids are reviewed. These studies cover a variety of turbulence modelling over different ranges of the fuel assembly.

2.1 CFD in Nuclear Engineering:

Spacer Grid Modelling: Spacer grids are mechanical structures placed periodically along the length of the reactor to provide stability to the fuel rods, maintain rod-to-rod clearance and reduce vibration in the fuel rods to some extent. Some spacer grids are designed such that they aid in turbulent mixing of the flow which improves heat transfer. These spacer grids have mixing vanes fitted on them which promote inter-subchannel flow which will promote local heat transfer by changing the local heat transfer coefficients. Hence studying the effects of spacer grids becomes very important. In addition of the crossflows, these structures also cause additional pressure losses which need to be accounted for. High-fidelity simulations have been conducted to study the complex flow patterns that are generated in fuel bundles using different turbulence modeling methods. Many CFD studies analyzed flow through mixing vanes in a Pressurized Water Reactor (PWR) assembly using Reynolds Averaged Navier Stokes (RANS) turbulence modes. Conner et al. (4), Gandhir and Hassan (5) modeled CFD methodology for a steady-state normal operation with renormalization group (RNG) k- ε turbulence model and validated with experimental data. Studies such as Bieder et al. (6) compared the performance of LES and RANS over a similar domain. It was observed that both the models could accurately predict the mean velocity profiles compared to experimental values. An interesting study by Busco and Hassan (7) applied Partially Averaged Navier Stokes (PANS) equation to the 5x5 domain with spacer grids. PANS is an energy based filtered representation of the Navier Stokes equations. The implicit

filtering approach enables the usage of PANS as a classical RANS, LES or even Direct Numerical Simulations (DNS) model without any change in the closure models. It was observed that PANS could predict the turbulent velocity profiles accurately compared to literature based on RANS and LES studies. The energy-based cut-off provided a chance to resolve the most importance large scale unsteadiness at minimal computational cost.

Heat Transfer: The cooling efficiency of the reactor core plays a key role in the safety of the nuclear power plants. In PWRs, the coolant flow is generally in a single-phase liquid form, although subcooled boiling may occur during normal operation at upper part of the hottest fuel assembly in the core. Boiling can lead to increase in the heat transfer as the water flows into the spots where the bubble leaves the rod surface. But when the heat flux increases over a certain value, the bubbles form layer of steam on the fuel rod which drastically decreases the heat transfer efficiency. In PWRs, this happens in the subcooled or low-quality regions. In case of Boiling Water Reactors (BWRs), this occurs in high steam quality region where flow pattern is annular and when rate of evaporation is high, dry patches appear on the fuel surface. This heat flux is called as the critical heat flux (CHF) and the boiling regime is called as boiling crisis. Fuel cladding is the first barrier which holds the fission products and hence its structural integrity is of utmost importance. Such extreme heat flux can lead to degradation of the cladding due to burn up and thermal stresses which eventually can lead to a rupture. Thus, the core should be properly designed to increase the CHF to the maximum extent and to maintain the reactor is operating below this value. Earlier CHF prediction studies were carried out on vertical heated tubes that don't include mixing vane spacer grids ((8)(9) (10)). Studies like Zhang et al. (11) and Xu et al. (12) show the application of Eulerian-Eulerian two-phase flow modelling to predict in CHF in a 5x5 and PWR assembly. Both studies included mixing vane spacer grids in the

geometry and were simulated using the CTF code FLUENT and the RNG k-epsilon model (13) and STAR-CCM+ (14). Saini and Bolotnov studied the effects of mixing vane spacer grids on dispersed droplet flow (15) using the DNS code PHASTA.

Reduced Order Modelling: Still simulations with LES and DNS are computationally very expensive. The study by Bieder et al. (6) had an element count of 300 million. A simple 5x5 rod study (16) without spacer grids with DNS modelling had a mesh count of over 8 million elements for Reynolds number of 19,000 which is fairly low mass flow rate. To reduce the computational cost that comes from the refined meshing, efforts were also made to remove the need for physically model the spacer grid. To do this, momentum source terms were designed which would replicate the flow effects which are caused by the mixing vanes on spacer grids. A study by Hu and Fanning (17) applies the momentum sources to a wire wrapped bundle. The source terms are modelled as forces in the tangential, normal direction to the wire. These forces are calculated based on the local velocity profiles, which make them self-regulating in nature and don't need excessive calibration. The crossflow velocities were compared with LES and experimental data. Another study by Capone et al. (18) uses velocities and Reynolds Stresses extracted from detailed meshes and then converts them into source terms for the momentum and turbulent equations. Study by Mikuz and Roelofs (19) shows momentum source application to specific sections of the subchannel that overlap with mixing vanes. In most of these simulations the RANS turbulence models were applied but even doing so the simulations were limited to assembly or partial assembly level. The latest study in this domain was conducted by Fang et al. (20) where momentum sources were designed and verified with LES studies over a range of Reynolds numbers. It was observed that the RANS models with the source terms were able to predict the time-averaged crossflow and pressure loss due to mixing vane spacer grids quite

accurately. The highlight of this study is that, once the momentum source modelling was validated for a 2x2 subchannel geometry, it was applied onto a full SMR core (consisting over ten thousand fuel pins) which makes this a milestone CFD study.

To model the macroscopic effects of turbulence, the flow profiles are averaged over a certain length in the subchannel. An averaged coefficient called the single-phase mixing coefficient is applied in subchannel codes that is used to account for the inter-subchannel momentum and heat transfer. Many authors have calculated mixing coefficients based on experimental data. One of the earliest studies were done by Rowe and Angle (21). For this study, laboratory experiments were performed to determine the turbulent component of mixing occurring in parallel subchannel that are interconnected. The experimental setup was such as to replicate light water operating conditions. The average mixing was calculated by monitoring the concentration of lithium, deuterium and tritium which was measured at subchannel exits. It was observed that the mixing without boiling is nearly proportional to the flow rate and has a small dependence on Reynolds number. Another experimental study by Rowe et al. (22) investigated the effects of flow channel geometry on fully developed turbulent flow. The purpose of this study was to understand crossflow mixing in rod bundle subchannels. For this study experiments were conducted in the Reynolds number range of 50,000-200,000 while considering pitch-to-diameter ratios of 1.25 and 1.125. Study by Rehme (23) reviewed experimental data of natural mixing between subchannel. From these experiments it was concluded that cyclic and almost periodic flow pulsations through the gaps of rod bundles was the reason for the mixing rates which was observed through the gaps and turned out to be independent of the gap width. A simple correlation was developed for a mixing factor which can be used as a good approximation for any gap geometry. There are several such studies through the years where the mixing coefficient

is presented as a function of the hydraulic diameter of the subchannel, gap width and Reynolds number.

The above studies didn't consider the effect of spacer grids and were conducted over bare bundles. For higher Reynolds number cases, the flow is turbulent but the change in velocity profiles created by spacer grids needs special modelling because of the forced mixing created due to the obstruction to the axial flow. Yao et al. (24) studied the effects of spacer grids on local heat transfer. The premise of this study was to study effect of straight and swirling grid spacers and their effect on heat transfer. In another experimental study by McClusky et al. (25) the axial development of swirling flow in rod bundle subchannels is presented. The swirling flow is generated by a split-vane pair located on the downstream edge of the support grid. By applying particle image velocimetry with an optical borescope, full-field lateral velocity data was obtained. Flow corresponding Reynolds number 28,000 was examined. It was observed from the lateral velocity fields that the swirling flows were first centered in the subchannel but with developing flow in the axial direction, the swirling shift from the center. An experimental by Shen (26) investigate the crossflow mixing effect caused by spacer grids fitted with mixing vanes. In this study detailed measurements of the transverse mean velocity and RMS velocity were obtained using the laser-Doppler velocimetry. For this study the rod had a pitch-to-diameter ratio of 1.375 and Reynolds number of 14,200. It was observed that the core flow downstream in the central subchannel with the promoter appears to be cylindrical vortex, but in the rod gap regions inversion of lateral velocity is encountered. It was also noted that the mixing rate from experimental studies varied largely with the angle of mixing blade on the grid spacer.

Apart from experimental studies, numerical methods, primarily CFD methods have been employed to capture the mixing effects of spacer grids. Ikeno (1) demonstrate application of

RANS methodology towards turbulence modelling of spacer grids in light water rod bundle subchannels. In this study the k-epsilon model was implemented to calculate the single-phase turbulent mixing coefficient by calculating the turbulent viscosity. Later the author notes that by using the k-epsilon model the details and effects of larger eddied was not accounted for and was rectified. Another study by Jeong et al. (27) demonstrate the turbulent mixing coefficient calculation in a KALIMER-600 design which is a sodium cooled reactor. Studies like Blyth and Avramova (2) (originally proposed in a study by Avramova (3)) demonstrate the offline coupling of CFD code with CTF. In this study the heat transfer enhancement and form pressure loss data are obtained from high fidelity STAR-CCM+ simulation and provided to CTF as parameters which greatly increase the predictive capability without sacrificing runtime efficiency. Another example of CFD informed analysis is provided in the study by Salko et al. (28) and Gilkey (29) where CFD informed CTF model is used to better account for spacer grid effects like, enhanced rod-to-fluid heat transfer, which influences crud growth and boron deposition calculations. CTF provides thermal feedback to coupled code VERA, which performs neutronics, TH and crud growth calculations for accurate prediction of power. In a study by Kulkarni et al. (30) preliminary grid loss coefficients were calculated at Reynolds number of 1,000, 5,000 and 10,000 for different spacer grids using Nek5000. Unstructured meshing was applied to non-mixing vane and mixing vane and structured meshing was used for simplified spacer grids.

CHAPTER 3: METHODOLOGY

3.1 The Spectral Element Method Code Nek5000

Nek5000 is a CFD spectral element method (SEM) code that can be applied towards simulating a variety of flow phenomenon. SEM is a subclass of Galerkin methods or weighted residual methods. It has low numerical dispersion and is non-dissipative in (31). Nek5000 is a weighted residual method which is known to combine the accuracy of spectral element methods and the flexibility of FEMs. The idea is to use Lagrangian interpolation on Gauss-Lobatto Legendre (GLL) quadrature. In doing so, the computational error with SEM goes down exponentially which leads to faster convergence compared to typical FEM. It features state-of-the-art, scalable algorithms that are fast and efficient on platforms ranging from laptops to the world's fastest computers. Applications span a wide range of fields, including fluid flow with incompressible and compressible, thermal convection, combustion, conjugate heat transfer and magneto-hydrodynamics. To model turbulence, Nek5000 is equipped with DNS, LES and in recent years, RANS capabilities.

To run a Nek5000 code the several input file which need to be modified based on the simulation. A brief summary of the files utilized for the Nek5000 simulations is mentioned below:

- **.par* – This file contains data for solution control like write interval, end time, time stepping method, LES control parameters etc. This file is also used to provide Reynolds number and Peclet number along with tolerances for the velocity, pressure and temperature solver.
- **.usr* – This file contains individual subroutines based on the tasks that need to be carried out. Subroutine for initial conditions, boundary conditions, boundary type information and also specific calculation that need to be carried out at each time step are defined here.

- **.re2* – This file contains the mesh data that will be read in the Fortran environment.
- **.ma2* – This file is generated for the mesh partitioning.
- *SIZE* – This file contains the data for the number of Gauss Lobatto Legendre (GLL) points to be used in each direction per-element. Based on the computational size of the problem, the minimum and maximum number of processors need to be specified here. Nek5000 has a functionality to specifying the pressure solver either as P_N-P_N or P_N-P_{N-2} which can be specified here.
- **.his* – This file contains all the probe points which are called as history points in Nek5000. These history points provide the interpolated flow field values for co-ordinates that are located in the geometry.

In this section a brief theoretical background of the CFD code Nek5000 is provided. This section covers the different conservation equations and their implementations in Nek5000. Further, conservation equations implemented in the subchannel code CTF are discussed.

Navier Stokes Equation

In this study only the incompressible flows with constant properties were considered. With these equations the mass, momentum and continuity equations can be written as follows:

$$\frac{\partial u_i}{\partial x_i} = 0 \tag{1}$$

$$\frac{\partial u_i}{\partial t} + \frac{\partial}{\partial x_j}(u_i u_j) = -\frac{1}{\rho}\frac{\partial P}{\partial x_i} + \frac{\partial}{\partial x_j}\left[v\left(\frac{\partial u_i}{\partial x_j} + \frac{\partial u_j}{\partial x_i}\right)\right] \tag{2}$$

$$\frac{\partial T}{\partial t} + u_j\frac{\partial T}{\partial x_j} = \frac{\partial}{\partial x_j}\left(\frac{v}{Pr}\frac{\partial T}{\partial x_j}\right) + \frac{\dot{q}}{\rho c_p} \tag{3}$$

Where u_i is the velocity vector, P is pressure, v is the kinematic viscosity, ρ is the density, T is temperature, c_p is the specific heat at constant pressure and Pr is the Prandtl number. Nek5000

has an option to scaled simulations for which the non-dimensional Navier Stokes is implemented (Equation 4). To non-dimensionalize the simulation, the geometry is scaled by the hydraulic diameter D_h. A major advantage of this simulation is that it takes less wall time compared to dimensional simulation.

$$\frac{\partial u_i^*}{\partial t^*} + u_j^* \frac{\partial u_j^*}{\partial x_j^*} = -\frac{\partial P^*}{\partial x_i^*} + \frac{1}{Re}\frac{\partial}{\partial x_j^*}\left(\frac{\partial u_j^*}{\partial x_i^*} + \frac{\partial u_i^*}{\partial x_j^*}\right) \tag{4}$$

The non-dimensionalization is carried out using the following non-dimensional variables

$$x^* = \frac{x}{D_h}; u^* = \frac{u}{U}; t^* = \frac{tU}{D_h}; P^* = \frac{P}{\rho U^2} \tag{5}$$

Similarly, the energy equation is non-dimensionalized as follows

$$\frac{\partial T^*}{\partial t^*} + u_j^* \frac{\partial T^*}{\partial x_j^*} = \frac{1}{Pe}\frac{\partial^{2*} T^*}{\partial x_j^{2*}} + q'''^* \tag{6}$$

The non-dimesionalization is carried out using the following variables

$$x^* = \frac{x}{D_h}; u^* = \frac{u}{U}; t^* = \frac{tU}{D_h}; T^* = \frac{T^* - T_0}{\Delta T_{ref}}; q'''^* = \frac{q''' D_h}{\rho c_p u_0 \Delta T_{ref}} \tag{7}$$

Large Eddy Simulations

The LES turbulence model has a higher fidelity than RANS in terms of accuracy of modelling but has also a higher computational cost associated with it. If the mesh and filter are correctly applied, then above 80% of the energy can be resolved in the domain. The basic principle of LES can be summarized in the following steps (32):

- A filtering operation is defined to decompose the velocity field u, into the sum of filtered component $\bar{u}$, and the residual or the sub-grid scale (SGS) component u'such that,

$$u = \bar{u} + u' \tag{8}$$

- The equations for the filtered velocity are derived from the Navier Stokes equation. These equations are of the standard form, with momentum equation containing the residual stress-tensor that arises from the residual motions.
- Closure is obtained by modelling the residual stress tensor, for example by using an eddy viscosity model.
- The filtered equations are solved for $\bar{u}$ which provides an approximation to the large-scale flow.

The general filtering operation is defined by

$$\bar{u}(x,t) = \int G(r,x)u(x-r,t)dr \tag{9}$$

Where the integration is over the entire flow domain and the specified filter satisfies the condition $\int G(r,x) = 1$.

The transport equation for the filtered velocity can be written as:

$$\frac{\partial \overline{u}_\iota}{\partial t} + \overline{u}_\jmath \frac{\partial \overline{u}_\iota}{\partial x_j} = -\frac{1}{\rho}\frac{\partial \bar{p}}{\partial x_i} + \frac{\partial}{\partial x_j}\left(v\frac{\partial \overline{u}_\iota}{\partial x_j}\right) - \frac{1}{\rho}\frac{\partial \tau_{ij}}{\partial x_j} \tag{10}$$

Where $\bar{p}$ is the filtered pressure field. This expression is different from the RANS equation because $\overline{u_\iota u_\jmath}$ is not the same as $\overline{u}_\iota \overline{u}_\jmath$. The residual stress tensor is defined by

$$\tau_{ij} = \overline{u}_\iota \overline{u}_\jmath - \overline{u_\iota u_\jmath} \tag{11}$$

And the anisotropic stress tensor is given by

$$\tau_{ij}^r = \tau_{ij} - \frac{2}{3}k_r\delta_{ij} \tag{12}$$

The high-pass filter in Nek5000 is based on a method described by Stolz et al. (33), is applied along with the LES turbulence model. This is another method of application for the sub-grid scale dissipation. In the HPF method, the convolution operator is used to obtain a low-pass

filtered signal. The high-pass filtered quantity is generated by subtracting the low-pass filter term from the original signal. For any given scalar, this term is represented as follows

$$X(u - \bar{u}) \tag{13}$$

Where u is the original signal and $\bar{u}$ is the low-pass filtered signal and X is a constant for proportionality. This is term is non-zero only for the last few Legendre modes, k>N' in a polynomial space. This term is subtracted from the momentum and energy transport equations respectively and represents the necessary energy drain from the discretized system.

$$\frac{\partial u_i}{\partial t} + \frac{\partial}{\partial x_j}\left(u_i u_j\right) = -\frac{1}{\rho}\frac{\partial P}{\partial x_i} + \frac{\partial}{\partial x_j}\left[v\left(\frac{\partial u_i}{\partial x_j} + \frac{\partial u_j}{\partial x_i}\right)\right] - X(u - \bar{u}) \tag{14}$$

$$\frac{\partial T}{\partial t} + u_j \frac{\partial T}{\partial x_j} = \frac{\partial}{\partial x_j}\left(\frac{v}{Pr}\frac{\partial T}{\partial x_j}\right) + \frac{\dot{q}}{\rho c_p} X(T - \bar{u}) \tag{15}$$

3.2 Subchannel Code CTF

Subchannel codes like CTF are lower fidelity codes which must be informed of the different physics by the means of parameters. These codes are computationally cheap compared to CFD codes. CTF uses a two fluid, three field modelling approach for two-phase flow in which the three fields are continuous liquid film, entrained liquid droplets and vapor. CTF uses a form of Semi-Implicit Method for Pressure-Linked Equations (SIMPLE) to solve the conservation equations. CTF has been extensively validated for PWR and BWR analysis and is widely used in multi-scale as well as multi-physics coupled calculations. Each field has a set of conservation equations with the assumption that the continuous liquid and the entrained droplet fields are in thermal equilibrium and thereby share an energy equation. To be used in a thermal hydraulic code environment, the conservation equations are discretized and then applied and solved over a mesh of finite volume. The mass conservation equation is as follows:

$$\frac{\partial(\alpha_k \rho_k)}{\partial t} + \nabla * \left(\alpha_k \rho_k \overrightarrow{V_k}\right) = L_k + M_k^T \tag{15}$$

Where α_k, $\overrightarrow{V_k}$ and ρ_k are the volume fraction, velocity field and density of the phase k. The first term on the LHS represents the change in mass over time and second term accounts for the advection of mass. On the RHS, the first term represents mass transfer in and out of a phase and the second term is mass transfer due to turbulent mixing and void drift. The momentum equation is written as follows:

$$\frac{\partial\left(\alpha_k \rho_k \overrightarrow{V_k}\right)}{\partial t} + \frac{\partial\left(\alpha_k \rho_k u_k \overrightarrow{V_k}\right)}{\partial x} + \frac{\partial\left(\alpha_k \rho_k \overrightarrow{v_k V_k}\right)}{\partial y} + \frac{\partial\left(\alpha_k \rho_k \overrightarrow{w_k V_k}\right)}{\partial z} = \alpha_k \rho_k \vec{g} - \alpha_k \nabla P + \nabla * \left[\alpha_k \tau_k^{ij}\right] + M_k^L + M_k^D + M_k^T \tag{16}$$

The first term of the LHS represents the change in momentum with time and the next three terms signify the advection of momentum in the three directions. On the RHS, the first and second term are the gravity and pressure force respectively. The third term represents the viscous shear force that accounts for the wall drag and form losses. The next three terms represent the momentum change due phase change, interfacial drag and turbulent mixing and void drift respectively. In this study we are considering only single-phase flows and hence the forces due to void drift, interfacial drag and phase change will not be discussed. The remaining two major forces are friction and form losses and turbulent mixing. Subchannel meshes are not as fine as CFD meshes, therefore cannot model the velocity profile accurately. The momentum changes due wall shear and turbulent mixing (wall heat transfer) need to be modeled as source or sink terms and are referred to as macro-mesh cell closure models.

Turbulent Mixing

In CTF, the turbulent shear stress is not modeled. Turbulent mixing is captured using a simple turbulent diffusion approximation. It is to be noted, the turbulent mixing only occurs in

the lateral direction and gaps orthogonal to the gap direction are not considered in the subchannel approach. Further, gaps cannot convect transverse momentum from and to one another because they don't "know" of each other's existence. Instead, transverse momentum simply "disappears" when it leaves a gap and goes into a channel (26). The transverse mass flow due to turbulent mixing in CTF is defined by

$$W_{ij}^{m} = \frac{\beta \bar{G}}{\overline{\rho_{mix}}}\left(G_{iz} - G_{jz}\right)A_{gap} \tag{17}$$

Where W_{ij}^{m} is the transverse mass flow due to turbulence, β is the mixing coefficient, $\bar{G}$ is the averaged mass flux between subchannel i and j, $\overline{\rho_{mix}}$ is the averaged density between subchannel i and j, G_{iz} and G_{jz} are the mass flux in subchannel i and j and A_{gap} is the cross-sectional area of the gap. Once the governing conservation equations are set up for a computational cell mesh of the flow geometry, they must be solved simultaneously using a numerical approach.

Wall Shear and Form Loss

The wall shear term in CTF is calculated as a combination of the form and friction losses as shown below.

$$\tau_{w,x} = \left[\left(\frac{dP}{dX}\right)_{form} + \left(\frac{dP}{dX}\right)_{fric}\right]\Delta X \tag{18}$$

$$\left(\frac{dP}{dX}\right)_{form} = \alpha_k \frac{K_x}{2\Delta X}\rho_k |U_k| U_k \tag{19}$$

$$\left(\frac{dP}{dX}\right)_{fric} = \frac{f_w G_x^2 \varphi^2}{2D_h \rho} \tag{20}$$

Where k is fluid phase, U is the velocity field, α_k is the volume fraction and K_x is the form loss coefficient which is either user-defined or calculated. G_x is the mass flux, D_h is the hydraulic diameter, f_w is the friction factor which is a function of Reynolds number and the surface roughness factor and φ is the two-phase multiplier.

3.3 Pressure Loss Across Spacer Grids

To compare the pressure losses across spacer grids three planar-averaging methods were implemented. These methods are varying in methodology and implementation. The three methods are discussed hereafter.

Thin-Volume Averaging

The first approach leverages the GLL points already available in Nek5000 to calculate the average pressure near a given plane. Structured meshes allow GLL points across an entire flow area to be located in a single plane, but this is not always true with an unstructured mesh. The planar location is accompanied by a small offset value that expands the interrogation zone into a thin volume centered at the planar location. For example, an offset of 0.05 units creates a thin volume of 0.1 units wide, as shown in Figure 1. This method interrogates all the GLL points that lie within this thin volume for a specified variable (pressure in this case), and the arithmetic mean is calculated from the interrogated values. As the offset value reaches a limit of zero, the thin volume becomes a surface. In this work, offset values between 0.05 and 0.4 were investigated in select PSBT subchannels. It is important to note that Nek5000 uses two separate meshes for its velocity and pressure solutions, and this work only interrogated the latter.

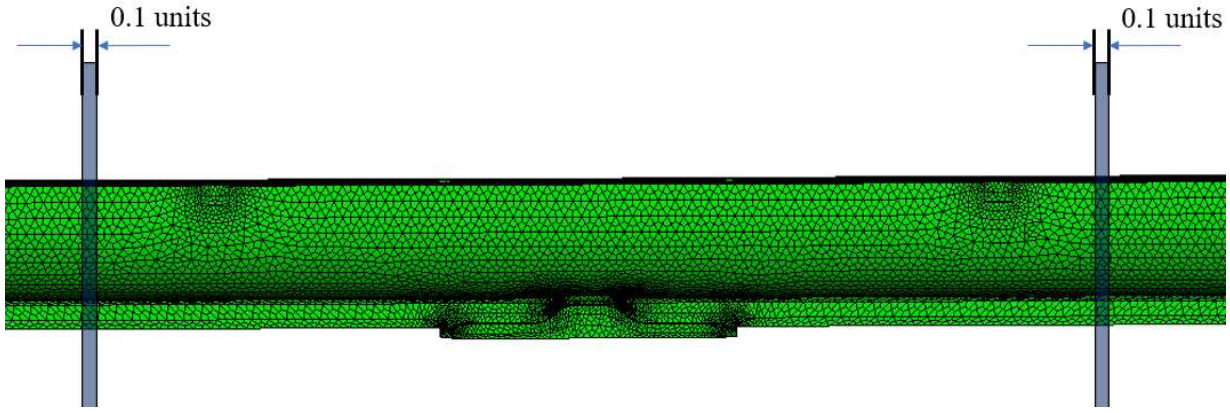

Figure 1. Thin volumes created by the offsets at the ends of spacer grid in a corner subchannel.

The thin-volume planar average was performed with a Fortran subroutine (34) which was called at every time step, and the average was appended to a data file in the working directory. This method requires minimal post processing, and the data are immediately available for all completed time steps. This subroutine can also be used to calculate planar averages at multiple locations and to obtain multiple offset values.

History Point Averaging

The second planar averaging approach used in this work was the averaging of history point data. Like many CFD programs, Nek5000 can extract point data from the solution field at any given time step. These points are referred to as history points in Nek5000, and their coordinates are provided as a *.his file in the working directory. In this analysis, history points were equally spaced at 0.02 space units in the span-wise directions over the cross-sectional flow area of each subchannel. Figure 2 illustrates the equally spaced history points in a side subchannel.

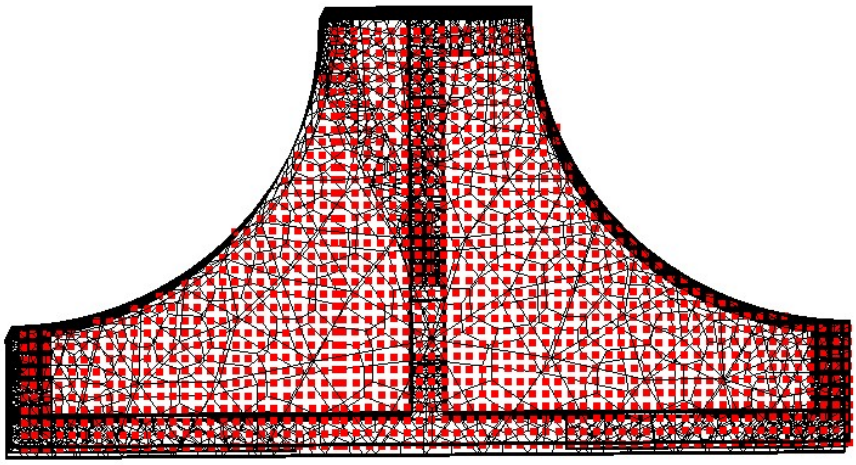

Figure 2. Depiction of history points in a side subchannel.

One set of history points was placed at each end of the spacer grid in each subchannel. After every write interval, the three velocity components, pressure, and passive scalars, were appended

to the *.his file. An arithmetic mean of the pressure of each plane was then calculated, and the grid loss coefficient was calculated using Eq. (19).

VisIt Post-Processing

The third planar averaging approach investigated in this work is implemented with VisIt (35), an open-source visualization utility which can be used to post-process data obtained from Nek5000. Plane slices are generated at the same locations that were used in the other averaging methods, and the arithmetic mean is performed on the extracted data. The process is straightforward and does not require any modifications to the Nek5000 user file or working directory.

3.4 Pressure Loss from Wall Friction

As indicated in Equation 19, the friction pressure drop is dependent on a parameter called the friction coefficient. Many expressions exist to estimate the friction coefficient across laminar and turbulent flows which are mentioned in the CTF theory manual (36). In this study the custom friction factor is utilized that is calibrated specifically calibrated for the subchannel geometry.

$$f = A + BRe^{C} \tag{21}$$

Where Re is the Reynolds number and A, B and C are dimensionless coefficients which can be calibrated for specific geometry. For this calibration study result from Nek5000 are utilized to calibrate the friction model in CTF using DAKOTA (37). The calibration steps are as follows:

1. A range of different Reynolds number need to be simulated to provide enough data points for calibration study. In this study Re = 8,000, 10,000, 12,000 are simulated in Nek5000. The mesh developed (Figure 3) is such that it can accommodate all the Reynolds number mentioned above with different level of p-refinement.

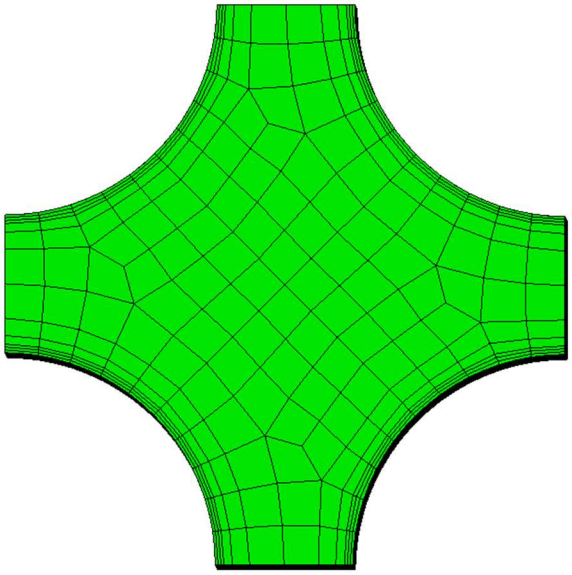

Figure 3. Mesh cross section of a bare center subchannel.

2. The length of the bare subchannel geometry is 100mm. Simulation in Nek5000 run much faster if they are non-dimensional. Therefore, the geometry is scaled by 9.5mm (diameter of the fuel rod) such that the mesh spans over -5.26 to 5.26 units in the y direction. The mesh is designed for flows up to Re = 15,000. The mesh has 34,160 hex20 elements and the min/max/average scaled Jacobians are 0.7, 0.9974, 0.9825 respectively.
3. To keep the computation cost low, the geometry length is limited to 100mm but this length is not sufficient for the flow to develop. Therefore, a recirculating boundary condition is applied from the inlet till halfway length. A subroutine developed by the Argonne National Laboratory (ANL) is available, which extracts the friction velocity. The sampling domain for this subroutine is kept from -5 to 0 units, which is roughly 50% of the geometry.
4. The calibration is done in NEAMS Workbench which has the capability of coupling DAKOTA and CTF. DAKOTA is used as a driver to run CTF for a range of values that are provided for the three coefficients. These coefficients need to be calibrated with the

friction velocity obtained from CFD results. The least squares method is used to check if the guess values from DAKOTA provided a better fit.

5. However, the friction velocity obtained from Nek5000 is dimensionless and CTF runs dimensional simulations. A Python script is run after each CTF run to calculate dimensionless friction velocity using the dimensional friction pressure drop the reported by CTF. The three coefficients are calibrated for five different flowrates. DAKOTA choses the best match for the coefficient value based on the least squares.

The DAKOTA-CTF coupling is here is done over two machines using the NEAM Workbench. The coupling and the simulation setup process is summarized below:

- NEAMS Workbench is installed on local machine and in the home directory of the RDFMG cluster at the North Carolina State University (NCSU). Depending on the operating system, generate SSH keys that will allow for logging into the remote cluster.
- **.setup* – This file contains the runtime commands which point to the python executables for DAKOTA on the remote connection and the file upload and download patterns. This file holds the remote login hostname and username.
- **.drive* – This file holds the information for point to the post-processing script that is used during calibration. This file also points to the SubKit executable in the directory; SubKit is preprocessor which is uses a simple input file to generate the CTF input deck.
- **.in* – This is the Dakota input file where the calibration methodology is selected and the remaining details are regarding initial guess, name of the calibration file etc. are specified.

3.5 Mesh Generation

The geometry and flow domains used in this work are adopted from the OECD/NEA PSBT Benchmark (38), which provides detailed descriptions of three different spacer grids. The benchmark has specifications for 5×5 fuel pin spacer grid geometries (Figure 4), but given the limited availability of resources, the current CFD studies were limited to the three different subchannels present in each type of grid. These subchannels are referred to as center, side, and corner for the remainder of this work. The subchannel extraction process was performed in Coreform Cubit 2020.2 (39).

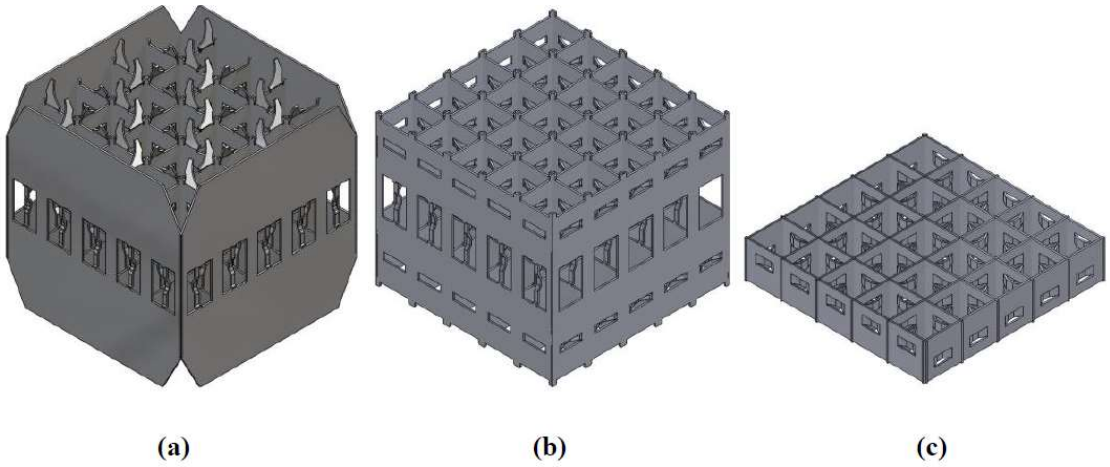

Figure 4. Three types of PSBT spacer grids: (a) Mixing Vanes Grids (MV); (b) Non-Mixing Vanes Grids (NMV); and (c) Simple Support Grids (SS).

The distance between mesh points must be within a certain limit to ensure the proper use of turbulence models. This limitation restricts both the thickness of the wall element layers on no-slip surfaces and the average cell size in the main flow region. These requirements can be met by using structured meshing, which is the process that was used to create the SS subchannels in this work. This process involved domain decomposition to allow direct sweep or mesh point mapping of each subdomain.

Nek5000 is a spectral element solver that requires HEX20 elements for computation. HEX20 are hexahedral elements with mid-side nodes. One way to ensure pure hexahedral element mesh is by applying structured meshing. But due to the complexity of the MV and NMV subchannels, structured meshes cannot be generated efficiently; therefore, unstructured meshes were used instead which consist of tetrahedral elements. A wide variety of tools are available for unstructured meshing. Previously, attempts were made to mesh the different subchannels in ANSYS ICEM as is demonstrated in the study (40). Figure 5 shows the complex geometry which includes the mixing vane, dimples and springs.

It is difficult to ensure a mesh only with tetrahedral and prism element meshes in such areas, and in such situations pyramid elements are used to fill the volume. Pyramid elements cannot be converted to hexahedral elements like tetra and prism elements, which makes the mesh inapplicable. Volumes made with offset surfaces were created so that first layer of boundary layer cell thickness corresponds to $y+ < 1$. These offset volumes can be created in Coreform Cubit 2020.2. The steps for creating individual subchannel geometries with boundary layer regions are shown below:

1. Import the spacer grid geometry file.
2. Create volume offsets around the spacer grid using surface offset tools.
3. Add fuel pins to complete the solid geometry.
4. Create volume offsets around the fuel pins and remove extra overlaps between the offsets.
5. Create a bounding box to represent the remainder of the fluid domain.
6. Subtract the solid grid and fuel pins from the bounding box.
7. Slice the bounding box at each pitch and extract the individual subchannels.

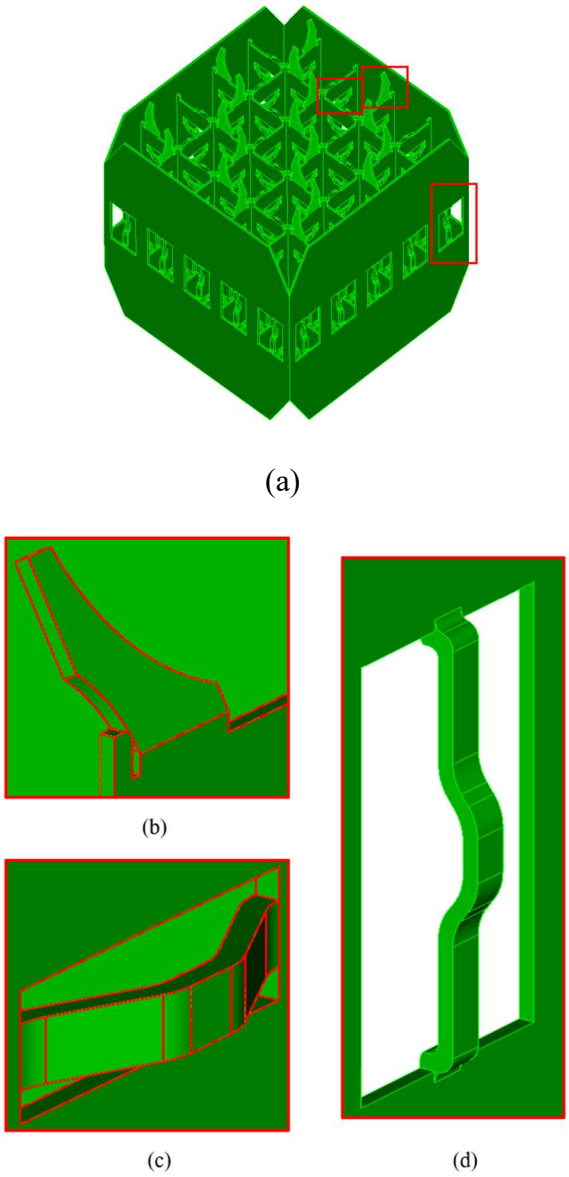

Figure 5. Components of the mixing vane geometry represented in Cubit: (a) 5x5 grid; (b) mixing vane; (c) dimples; (d) springs.

Once this process was complete, each subchannel had separate volumes for each boundary layer around the fuel pin, the spacer grid, and the bulk fluid region. These volumes were then meshed separately to control the maximum size of the elements, starting with the fuel offset volume. The following steps were used to generate the final HEX20 mesh required by Nek5000:

1. All surfaces were imprinted to ensure a conformal mesh.
2. The tetrahedral meshing tool was used with the auto-sizing functions, which led to the coarsest mesh in the free volume, and finer elements were placed in the proximity areas.
3. A HEX8 mesh was created from the TETRA mesh using the *thex* command, which breaks down each tetrahedral element into four hexahedral elements.
4. Node-projection was activated before converting the hexahedral elements into HEX20 elements which generates mid-curve nodes on the hexahedral elements. This step is crucial as the mid-curve nodes are projected to the geometry which leads to accurate capture of curvature for high-order elements.

The entire meshing process was completed in Cubit, and each mesh was exported as an EXODUS-II (*.*exo*) file. For the simulation, the *.*exo* file was converted to *.*re2* file using the *exo2nek* mesh converter tool. The offset volumes were generated using 0.2 and 0.4mm thicknesses for the fuel and spacer grid regions, respectively. These dimensions correspond to two and four layers of cells in the offsets around the solid surfaces and act as boundary layer cells. Smaller offsets of 0.1–0.3mm around the spacer grid structure resulted in much higher element counts or negative scaled Jacobians after element conversion because of low tetrahedral element thickness. Select mesh parameters for the nine subchannels meshed for a Reynolds number ranging up to 10,000 are listed in Table I.

Table 1. Mesh statistics for Re = 10,000

Geometry	Hex Elements	Scaled Jacobian (41) Avg/Min/Max
SS corner	53,711	0.8248/0.1736/1.0
SS side	135,278	0.7928/0.3652/1.0
SS center	72,280	0.7508/0.3938/1.0
NMV corner	176,412	0.4455/0.006037/0.7410
NMV side	358,204	0.4373/0.05248/0.7398
NMV center	451,420	0.4359/0.01676/0.7401
MV corner	93,281	0.4540/0.05535/0.7573
MV side	305,288	0.4261/0.02756/0.7399
MV center	436,460	0.072/0.0016/0.167

3.6 Hi2Lo Setup

Due to high computational cost, the SS center-center geometry is chosen for the mixing coefficient, grid enhanced heat transfer and lateral convection factor. The geometry (Figure 6) under consideration is still small considering only two hydraulic diameter of flow region for downstream. To avoid inlet effects, the geometry was extruded for a length of five hydraulic diameters upstream of the spacer grids. This region was used to implement the recirculating boundary condition to have a flow void of inlet effects as it reaches the spacer grid region. This center-center SS configuration has 121,278 Hex20 elements. The flow rate for these simulations is limited corresponding to Re = 10,000.

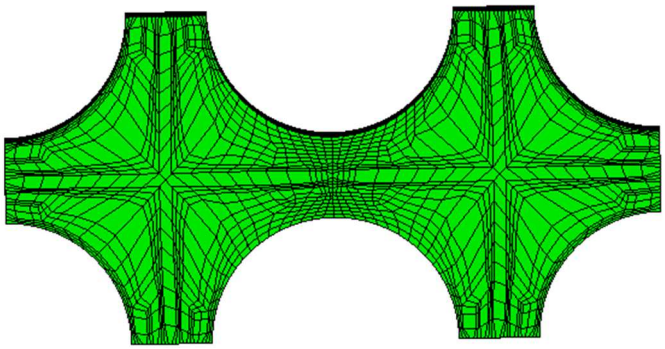

(a)

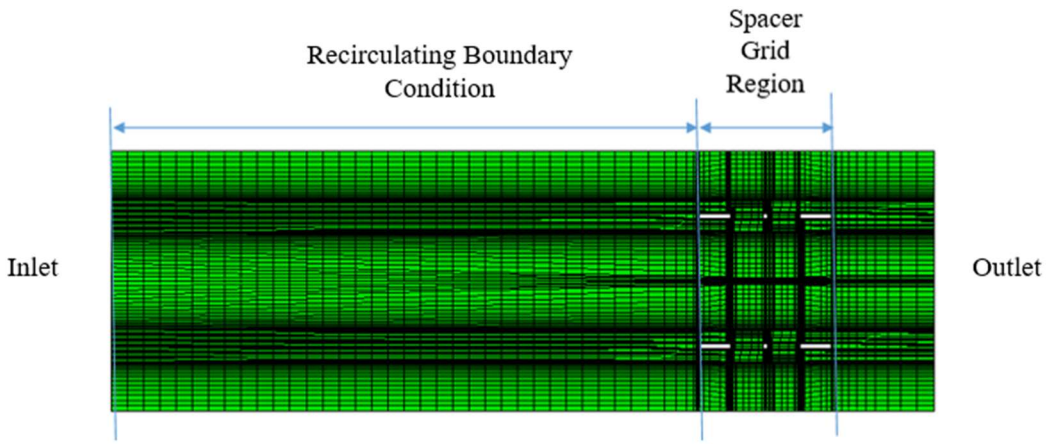

(b)

Figure 6. SS center-center configuration: (a) cross-section (b) longitudinal view.

3.7 Mixing Coefficient

Due to the presence of spacer grids, crossflow will be generated in the subchannels. This causes mixing of flows which needs to be calculated for accurate overall heat transfer calculations in CTF. Previously, this work has been done by Blyth and Avramova (2) . The mixing coefficient is given as follows

$$\beta = \frac{transverse\ flow}{axial\ flow} \tag{21}$$

Each subchannel, in the center-center configuration, namely i and j, is supplied with a different inlet temperature. Due to the turbulent nature of the flow, there will be a transverse mixing of

flow. For this simulation one subchannel is subject to inlet temperature of 300°C and the adjacent subchannel is subject to 310°C flow. This transverse flow is quantified by obtaining the temperature gradient across the gap. Temperature data will be extracted by placing the history points (Figure 7) on either side of the gap. Based on study by Blyth and Avramova, the offset gap was decided to be 0.1mm on either side of the gap.

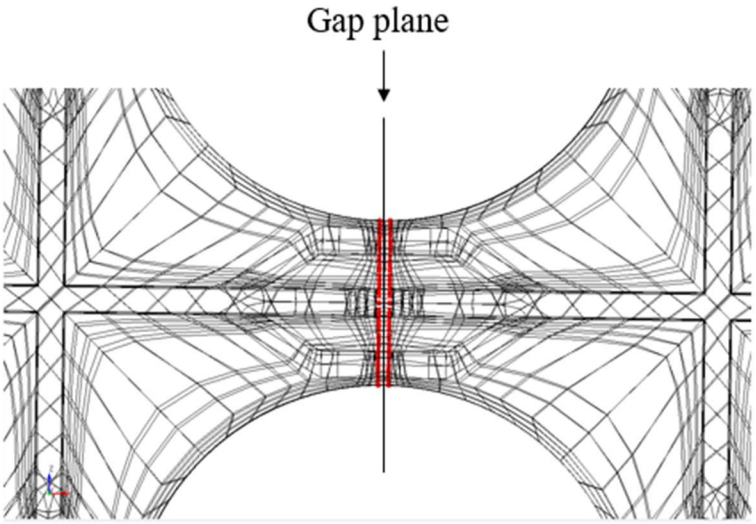

Figure 7. History points (in red) located at 0.1mm distance away from the gap.

$$T_{gradGap} = \frac{T_i(z) + T_j(z)}{2\Delta x_{gap}} \tag{22}$$

The effective heat flux acting at the gap is then calculated utilizing the volume-averaged values for specific heat of subchannel i. Equation 23 gives the procedure for determining the gap heat flux based on the thermal gradient.

$$q''_{gap}(z) = \frac{c_{p,i}}{Pr_{turb}} T_{gradGap}(z)\mu_{gap}(z) \tag{23}$$

Where $\mu_{gap}(z)$ is the average turbulent viscosity across the gap. The turbulent mixing coefficient is given as below

$$\beta = \frac{q''_{gap}(z)}{\left[T_i(z) - T_j(z)\right] c_{p,i} U_{in} \rho_i} \tag{24}$$

For calculating the turbulent viscosity, two major subroutines are implemented. The first subroutine called *budgets_avg*, needs to be called at all the write intervals by placing it in the *userchk* in the **.usr* file. This will write all the different "ingredient" terms such as root mean square (RMS) velocity, the three components of time averaged velocity etc. as field files along with the velocity and temperature data at each write interval. Once the simulation is complete, the second subroutine *ke_budgets* is called in a post-processing run. To run the simulation in post-processing run the *endTime* in the **.par* file should be changed to 0. The *ke_budgets* will just execute the subroutine in *userchk* without progressing with the simulation. *Ke_budgets* will read all the field files for the "ingredient" terms and apply time averaging to it. Once the time-averaged terms are available, different quantities can be calculated such as variance, covariance, dissipation etc. are calculated. For extracting this turbulence parameters across the gap history points are utilized. Currently, the history points subroutine only writes out the three velocity components, pressure and temperature. Thus, an alternate subroutine is created *hpts_tke* which uses the same setup as the history point subroutine but extracts the turbulent parameters needed. This subroutine is executed in the post-processing step after *ke_budgets*.

3.8 Grid Enhanced Heat Transfer

The setup for this measurement is rather simpler. Uniform inlet temperature is provided, and uniform heat flux is applied to the fuel surfaces. The wall temperatures will be extracted with history points (Figure 8) and the bulk temperatures will be extracted using planar averaging technique.

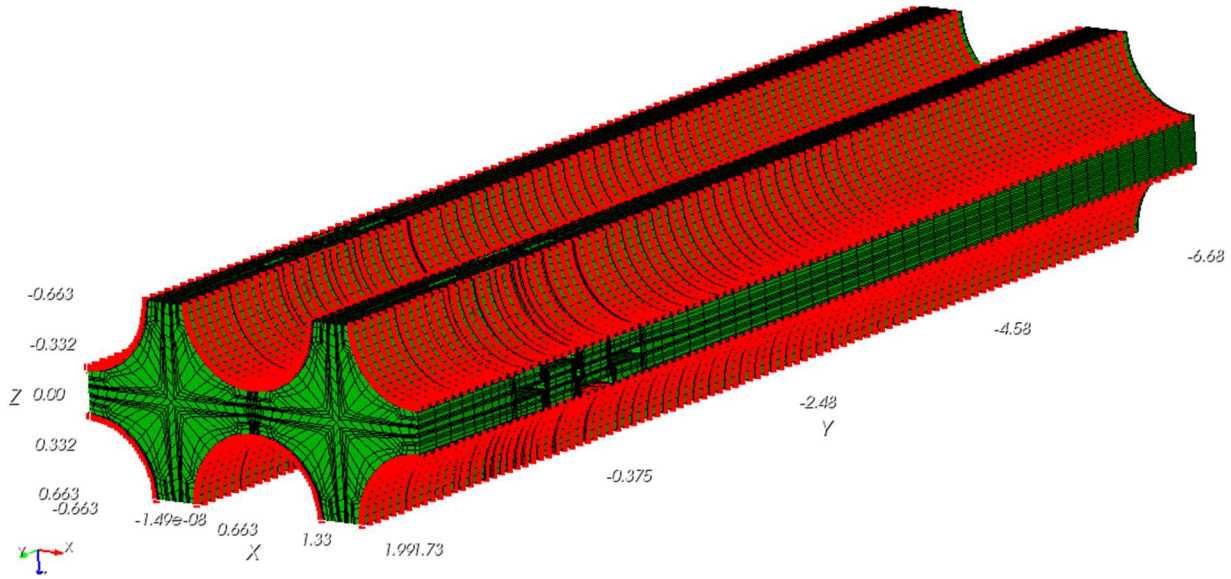

Figure 8. History points (in red) along the curved surfaces evenly located along the axial length

$$h = \frac{q''}{T_w - T_b} \tag{25}$$

$$f_{HTC} = \frac{HTC_{gridded}}{HTC_{bare}} \tag{26}$$

The heat transfer coefficient will be calculated for the spacer grid subchannels and for bare subchannels. Their ration will the multiplication factor which can be applied CTF for accurately estimating the heat transfer in subchannels.

CHAPTER 4: DISCUSSIONS OF THE OBTAINED RESULTS

In this chapter results pertaining to grid loss coefficients are presented for subchannels with MV, NMV and SS subchannels for the history point and thin-volume averaging method. The friction velocities and the resultant calibration is presented for a range of Reynolds numbers and polynomial order.

4.1 Validation at Laminar Flow

Nek5000 is applied in the non-dimensional format for the simulations in this study due to faster computational time. For preliminary validation of the code, a simulation conducted on a simple pipe geometry with length of 10 hydraulic diameters to obtain the typical Poiseulle flow profile at Reynolds number of 1,000 which is provided as an entry in the *.par file in Nek5000. The velocity contour and profile are shown in Figure 9.

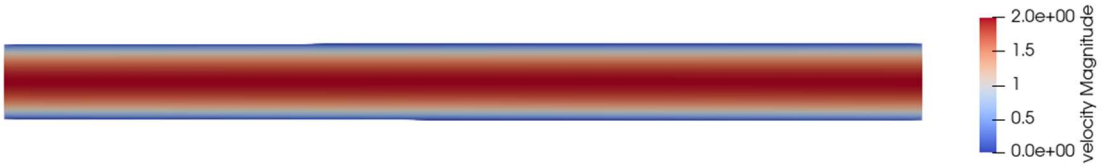

(a)

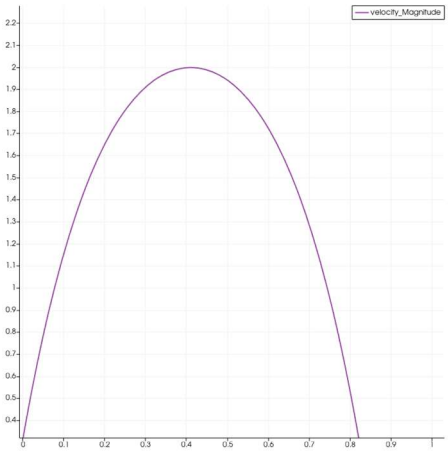

(b)

Figure 9. Laminar flow (a) velocity contour and (b) velocity profile as observed in a pipe geometry.

The simulation in this case was run for over 100 time units so as to make sure the velocity profile had reached steady state. For applying the non-dimensional heat transfer the Peclet number needs to be provided in the *.par file along with the Reynolds number. Previous references are not found on the implementation of non-dimensional heat transfer and the user guide also lacks enough detail in this regard. In the previous section, the non-dimensional heat equation and the wall flux is demonstrated. For this simulation a same pipe geometry is considered, and a constant wall heat flux is applied to the wall. In this simulation a fully developed flow field is used as an initial condition. For post-processing, the thin-volume planar-averaging method is applied. To properly take into account the effect of low velocity regions near the wall, the following formulation is used for the temperature extraction.

$$T_{bulk} = \frac{\int u * T \, dA}{\int u \, dA} \tag{27}$$

Results from Nek5000 agree well with theoretical results for a laminar case of Re = 1,000. Figure 10 shows the re-dimensionalized result for temperature rise with varying inlet temperatures.

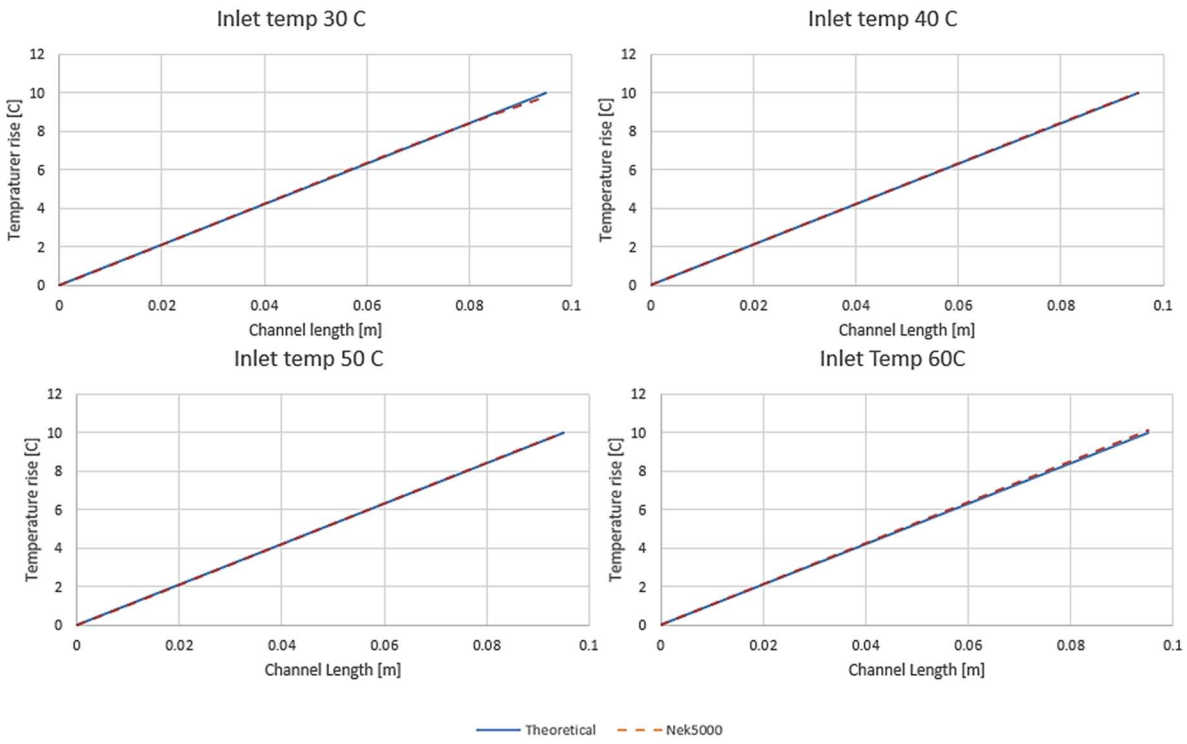

Figure 10. Re-dimensionalized temperature rise for laminar flow in circular pipes.

4.2 Pressure Losses

This section presents the grid loss coefficients from Nek5000. In this grid loss coefficient by post-processing the pressure drop across various subchannels in MV, NMV and SS. These results Figure 11 shows the grid loss coefficient for the MV corner subchannel vs. non-dimensional time. Since all simulations presented in this work are nondimensional, time here is measured in convective units. This plot shows a very good match for the two planar averaging method, as both variables overlap each other.

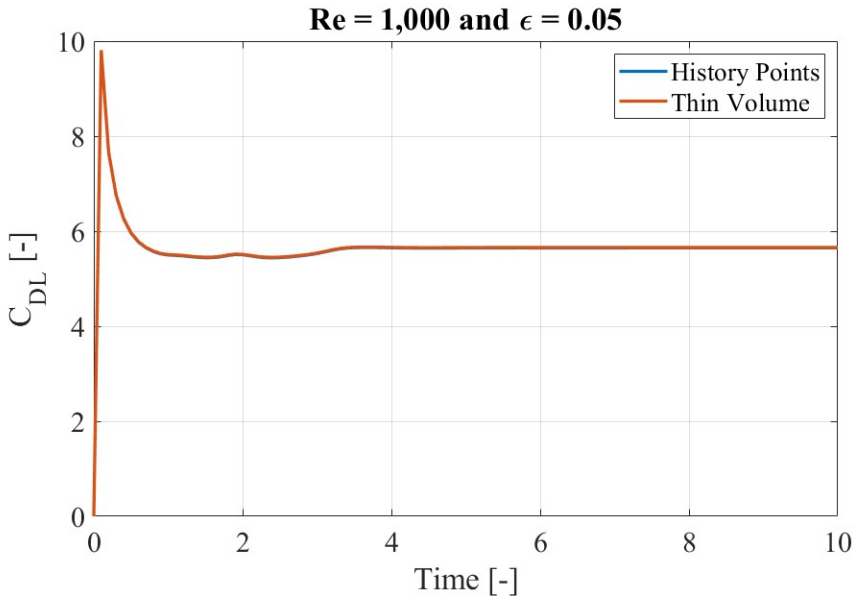

Figure 11. Grid loss coefficient for MV corner subchannel at Re = 1,000.

The corner simulation was run for 10 time units at Re = 1,000, and the grid loss coefficient remained stable with time. The flow appears to remain attached and laminar, which is expected at this Reynolds number.

Using the flow field at the last time step as the initial condition, the simulation of the MV corner subchannel was restarted at Re = 10,000. The plot for this grid loss coefficient is shown in Figure 12. Again, both the thin-volume and history point approaches follow the same trends, and the results agree quite well with each other. The value of loss coefficient also drops significantly, which is expected as the flow rate increases. The results between t = 0 and 1 convective units are not presented due to their large swings after restarting the simulation. This result is not uncommon when the inlet condition is many times larger than the initial field conditions, but this technique is still attractive for complex domains.

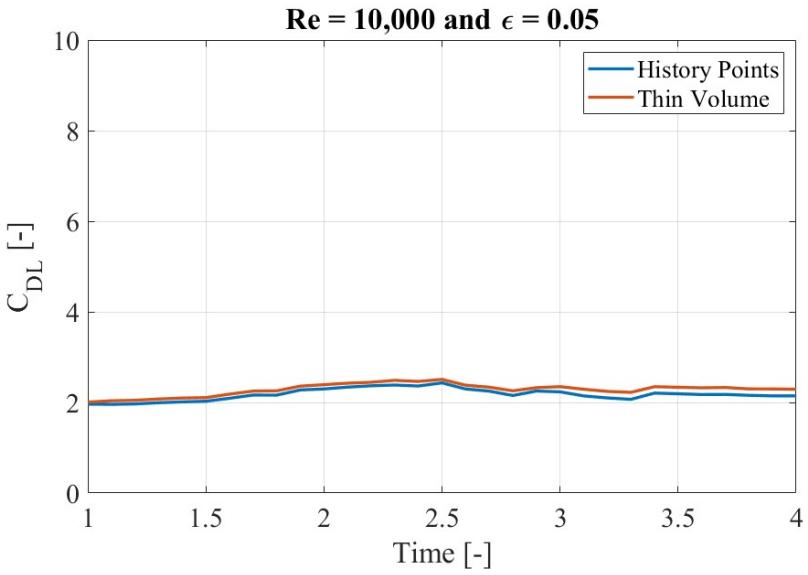

Figure 12. Grid loss coefficient for MV corner subchannel at Re = 10,000.

Figure 13 shows grid loss coefficient for NMV center subchannel, in which both techniques agree well and seem to be approaching convergence over time. These trends are similar to the ones observed in Figure 11 for the MV corner subchannel.

Figure 14 shows grid loss coefficient for the NMV corner subchannel. Even though the flowrate is in the laminar domain there is difference in prediction between the two methods. The plot overlaps till 0.2 time units and then offsets with the history points underpredicting the grid loss coefficient by 12.32% with respect to the thin volume approach. This might be due to some odd mesh elements in the geometry near the spacer grid region. To get a better understanding for this deviation, a mesh sensitivity and epsilon sensitivity can be conducted. In the MV corner case, the coefficient starts to stabilize only after 4 time units, and the same can be expected with the NMV corner case with longer simulation.

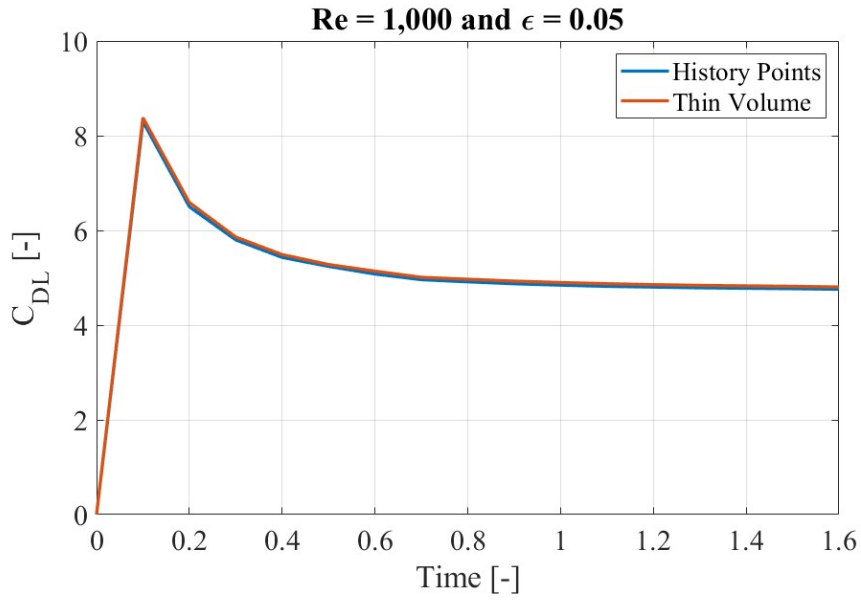

Figure 13. Grid loss coefficient for NMV center subchannel at Re = 1,000.

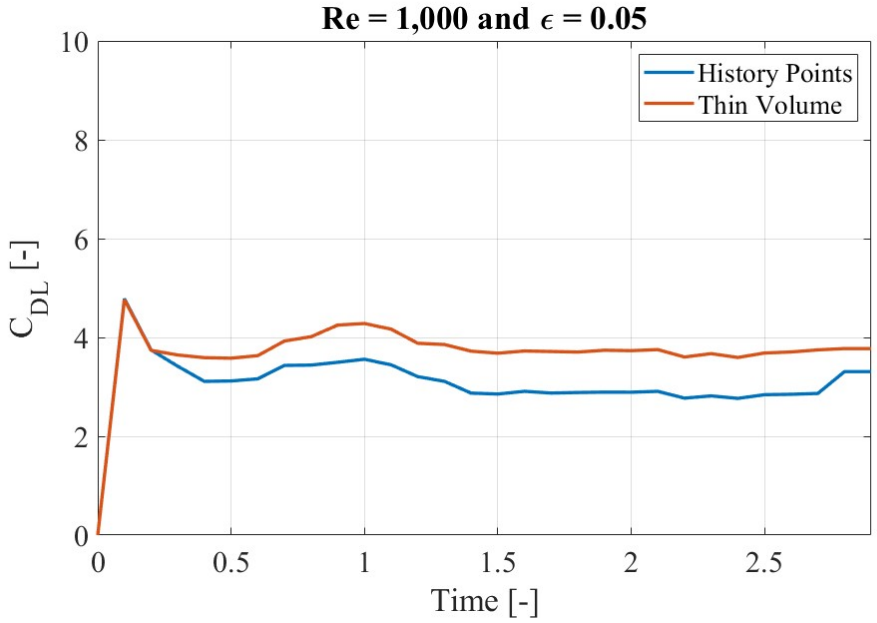

Figure 14. Grid loss coefficient for NMV corner subchannel at Re = 1,000.

The results for the grid loss coefficients with individual subchannels have been summarized and presented in Table 2. The best agreement can be seen for the MV corner subchannel at Re = 1,000 followed by Re = 10,000. Results from the NMV center and the MV

center are also quite close, predicting within 1% with respect to either value from either approach.

Table 2. Grid loss coefficients comparison from the two methods used in the MV and NMV subchannels

Geometry	**Reynolds Number**	**T_{FINAL}**	**History Points C_{DL}**	**Thin Volume C_{DL}**	**Absolute Difference**
MV corner	1,000	10.0	5.648	5.658	0.01
MV corner	10,000	4.8	2.305	2.348	0.033
NMV corner	1,000	2.9	3.308	3.773	0.465
NMV center	1,000	1.6	4.757	4.805	0.048
MV center	1,000	1.0	5.074	5.117	0.043

To enhance understanding of the history point calculation, some statistics about the history points are presented in Table 3. Maximum standard deviation in the results can be seen for the plane after the spacer grid in the NMV corner subchannel, even with same number of history points and the same flowrate as that for the MV corner. This could suggest that the cause of this prediction irregularity could be related to mesh having high aspect ratio elements near the plane of consideration.

Similar methodology was applied for investigating the pressure drop in the SS subchannels. For this study multiple plane groups were investigated as represented in Table 4. The first plane group is based at the ends of the solid spacer grid boundary and the subsequent plane groups are placed further and further away from the preceding plane.

Table 3. Statistics for nondimensional pressure calculated from history points

Geometry	Reynolds Number	Last time Step in Convective Units	Number of Grid Points per Plane	Plane after Grid: Mean/ Standard Deviation	Plane before Grid: Mean/ Standard Deviation
MV corner	1,000	10.0	682	0.4292/0.0709	2.8267/0.0231
MV corner	10,000	4.8	682	-0.0034/0.2024	1.0998/0.0229
NMV corner	1,000	2.0	682	-0.1994/0.6460	1.4546/0.0857
NMV center	1,000	1.6	2,589	-0.1360/0.0187	2.2428/0.2586
MV center	1,000	1.0	2,589	0.0649/0.1091	2.6022/0.2973

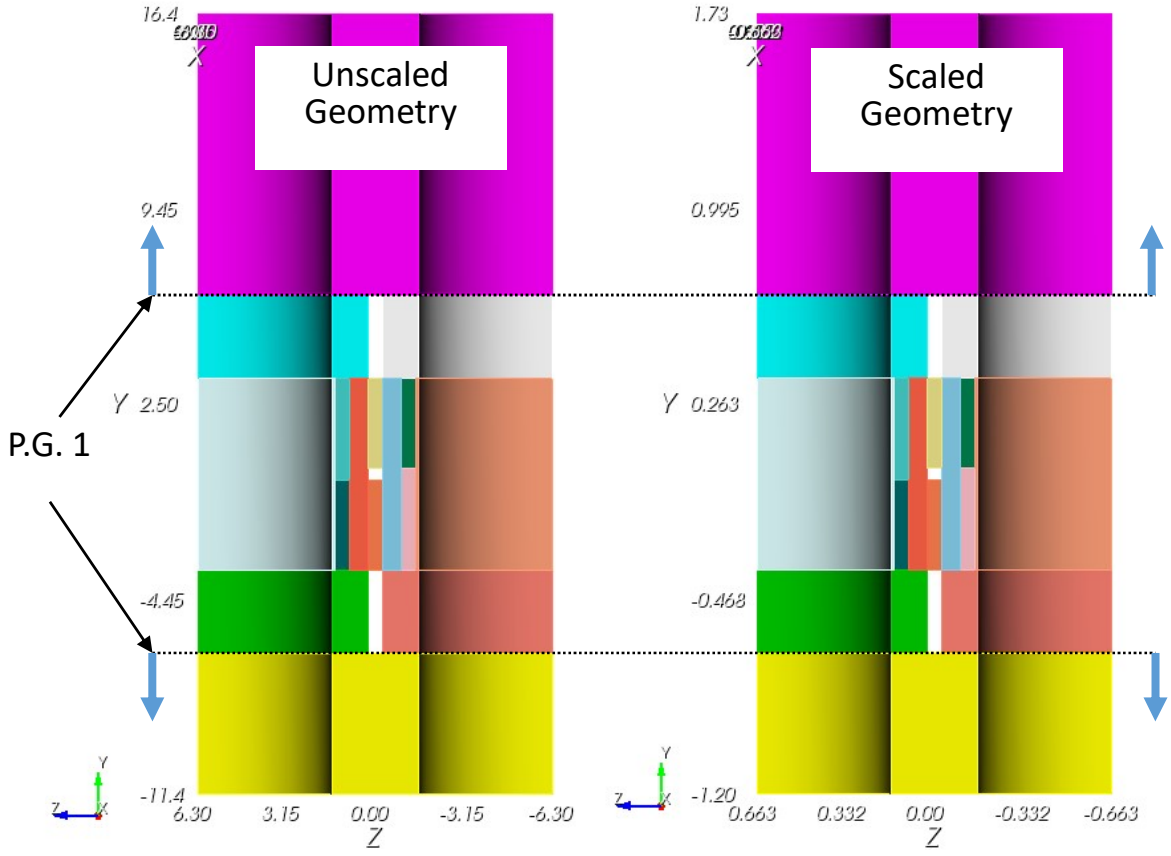

Figure 15. Plane locations in the SS subchannels.

Table 4. Unscaled and scaled plane locations used in SS subchannel simulations

Plane group (PG)	Unscaled plane Y-locations	Scaled plane Y-locations
1	-6.4, 6.4	-0.673683, 0.673683
2	-6.495, 6.495	-0.683683, 0.683683
3	-6.59, 6.59	-0.693683, 0.693683
4	-6.685, 6.685	-0.703683, 0.703683
5	-6.78, 6.78	-0.713683, 0.713683

The time history results of pressure loss coefficient for the center SS subchannel are illustrated in Figures 17 for Re = 10,000. Here, pressure loss is calculated via the thin-volume approach only, and the volume thickness (ε) of 0.01. In this figure the results between 0 and 2.0 time units are excluded as it contains the initial instability that are noticed when the simulation is started. Overall, good convergence is obtained in the results presented. As is expected, the pressure drop from Plane Group 1 is the least as the distance between the two plane groups is the minimum here. As the distance between the plane groups increases, the pressure loss coefficient increases, and larger pressure losses are accounted for.

The comparison between the different methods was done in a study by Kulkarni et al. (30) and Tables 4 and 5 summarize these results as obtained for a SSG subchannel. These data points were taken at the same point in time (10 convective units), and the disagreement between history points and VisIt is likely due to the number of samples taken. Approximately 20,000 and 50,000 samples were available for each plane in VisIt for Reynolds numbers of 1,000 and 5,000, respectively. Only 2,589 history points were used for each plane, and this was held constant between flow conditions.

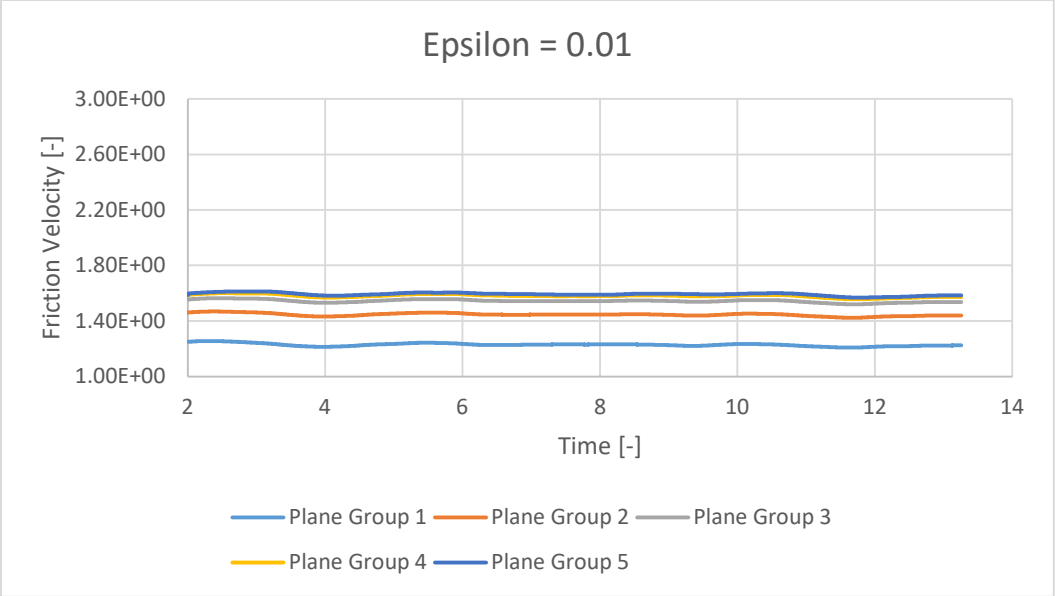

Figure 16. Pressure loss coefficient calculated with thin-volume approach for center SS subchannel.

Table 5. Comparison of the pressure loss coefficient in the center SS subchannel between history point and post-processing in VisIt

	Re = 1,000		**Re = 5,000**	
Plane Group	**History Points C_{DL}**	**VisIt C_{DL}**	**History Points C_{DL}**	**VisIt C_{DL}**
1	2.6389	2.2667	1.5805	1.2323
2	2.7737	2.7284	1.6961	1.7765
3	2.8524	2.8422	1.7658	1.8336
4	2.8944	2.8933	1.7987	1.8505
5	2.9117	2.9178	1.8124	1.8500
6	2.9166	2.9828	1.8177	1.8436
7	2.9216	2.9279	1.8183	1.8314

Table 6. Pressure loss coefficient results for the center SS subchannel via the thin-volume approach. The volume thickness (ε) was varied between 0.05 and 0.4.

		Re = 1,000				**Re = 5,000**			
Plane Group		ε = 0.05	ε = 0.1	ε = 0.2	ε = 0.4	ε = 0.05	ε = 0.1	ε = 0.2	ε = 0.4
	1	2.5532	2.5594	2.5410	2.4813	1.4984	1.4961	1.4783	1.4479
	2	2.6749	2.6319	2.5825	2.5068	1.6199	1.5642	1.5099	1.4590
	3	2.7783	2.6988	2.6219	2.5312	1.7180	1.6258	1.5398	1.4694
	4	2.8522	2.7581	2.6590	2.5546	1.7829	1.6787	1.5678	1.4791
	5	2.8949	2.8082	2.6935	2.5771	1.8144	1.7215	1.5934	1.4882
	6	2.9152	2.8478	2.7255	2.5987	1.8227	1.7529	1.6162	1.4965
	7	2.9225	2.8768	2.7542	2.6192	1.8189	1.7723	1.6362	1.5043

The disagreement of the thin-volume approach for higher thicknesses suggests that the volume thickness should be kept small for this domain. The pressure loss coefficient fluctuates slightly, but time-averaging will not improve the results much for Re = 1,000, where the main flow region is still well attached. Figure 12 compares the overall velocity magnitude contour and immediately downstream of the grid structure in the center SS subchannel for flow conditions of Re = 1,000 and 5,000 at 10 convective units in time. The separation occurring at Re = 5,000 is apparent and will only increase with higher Reynolds numbers. Verification at higher Reynolds numbers will require time averaging and possibly more convective units. Due to limited computational resources, the remaining cases are still being investigated.

4.3 Calibration of the Friction Coefficient

For the friction coefficient calibration flow corresponding Reynolds number of 8,000, 10,000 and 12,000 are simulated in Nek5000. It was originally found that the flow exhibited laminar characteristics even at Reynolds number of 20,000 as shown in Figure 9. Due to this reason, the friction velocities for different flowrates attained a stable value (Figure 19) after a while which is typical of laminar flow behavior.

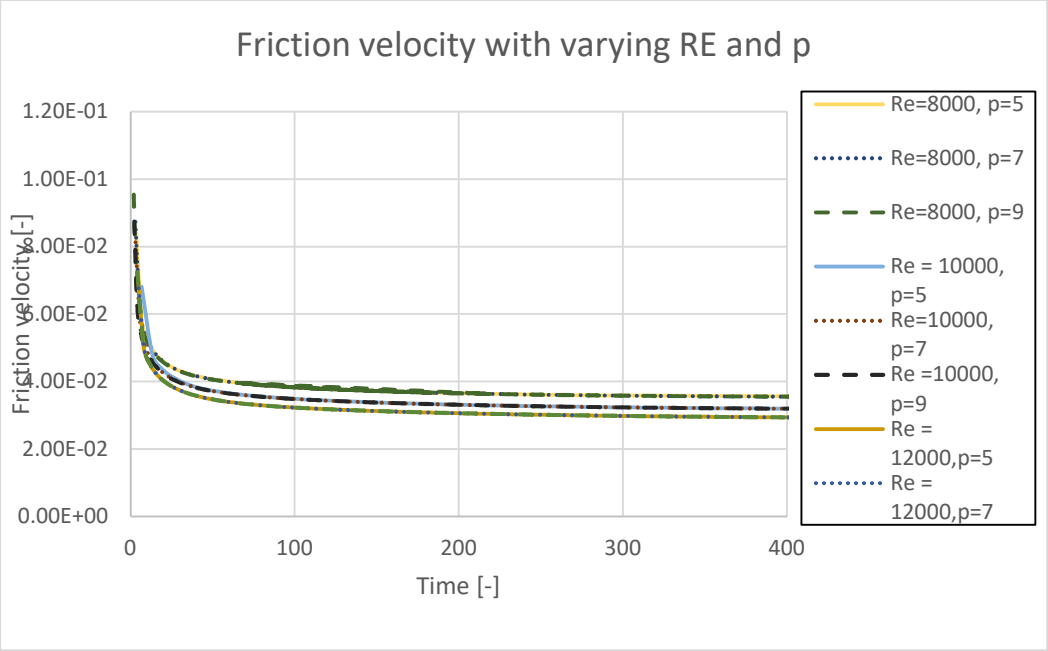

Figure 17. Friction Velocities with varying Reynolds number and polynomial order 'p'

To overcome this issue, turbulence needed to be artificially triggered in the simulation by adding instabilities to the flow field in the form of initial conditions. These perturbations trigger the turbulent eddies, and the Reynolds number is high enough to sustain the turbulence. The turbulent velocities for Reynolds number of 8,000 are shown in Figure 20. The flow was run for 10 flow-throughs to remove the inlet effects.

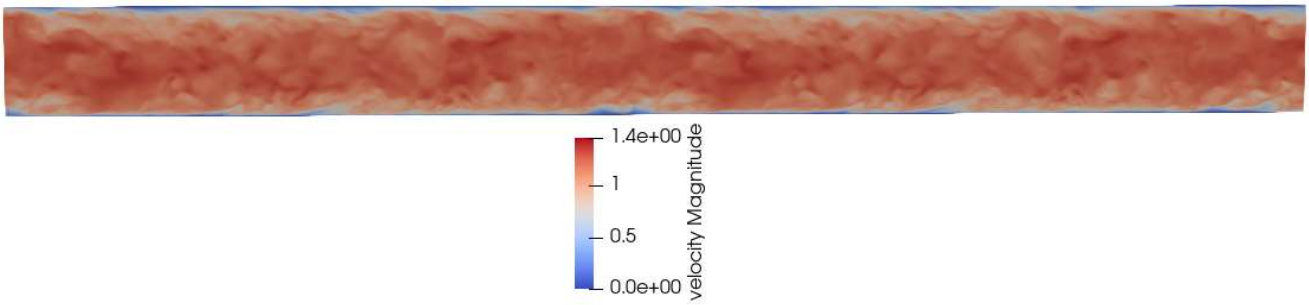

Figure 18. Turbulent non-dimensional velocity contours at Re=10,000.

These perturbations were applied to all the flowrates with varying polynomial order simulations and friction velocities were extracted as shown in Figure 21. The general trend observed with these simulations is a sharp decrease in the friction velocity after starting the simulation. Then depending on the Reynolds number, the friction velocity increases with time and eventually reaches, what could be describes as, a fluctuating plateau. This fluctuating friction velocity profile is indicative of developed turbulent flow.

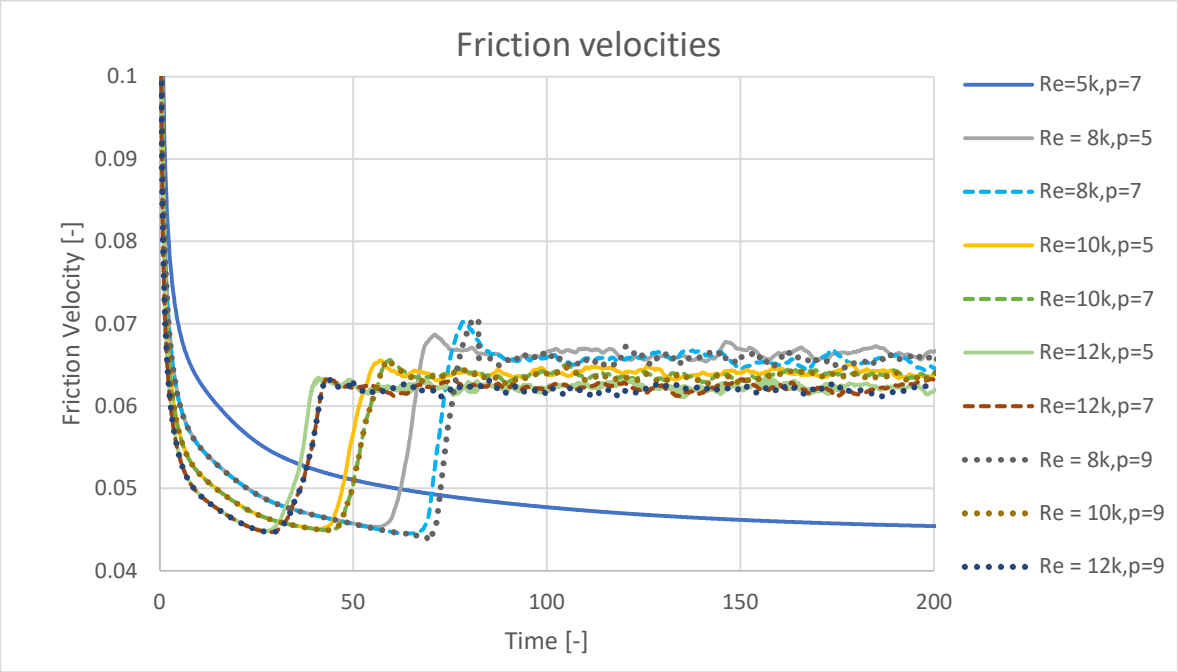

Figure 19. Friction velocities for flows with perturbations with varying Reynolds number and polynomial orders.

To demonstrate that the perturbation initial condition is not just causing the fluctuating friction velocity as plot of Reynolds number 5,000 is also added to Figure 21 which was initiated with the same initial conditions as the other turbulent flows. However, it can be observed that the friction velocity still followed the same trend as observed in Figure 19 and exhibit laminar behavior.

These friction velocities are time-averaged from 100-200 time units and provided as entries for the calibration file in DAKOTA as shown in Table 7.

Table 7. Time-averaged friction velocities for different Reynolds numbers and polynomial orders.

Reynolds Number	**P=5**	**P=7**	**P=9**
8,000	0.066181	0.065602	0.065602
10,000	0.064141	0.063891	0.063642
12,000	0.062252	0.062282	0.062312

Calibration simulation was carried out for each set of values for each polynomial order. For this simulation it was observed that coefficient A reaches zero in the first couple of iterations. Hence for reducing computation time coefficient A is set to zero and only B and C are calibrated over these input values. The calibrated B and C coefficients obtained for these simulations are presented in Table 8.

Table 8. Calibrated B and C coefficients for varying polynomial order.

Polynomial Order 'P'	**Coefficient B**	**Coefficient C**
5	0.141514	-0.31879
7	0.094062	-0.27505
9	0.071916	-0.23658

These calibration for different refinement of the mesh show variation in the calibrated coefficient B and C and thus will have uncertainty in the friction pressure drop prediction. Thus, this can be treated an uncertain input for CTF in the Hi2Lo coming from the mesh-based uncertainty in Nek5000. An uncertainty quantification analysis was attempted using DAKOTA. For this a Latin Hypercube Sampling (LHS) was implemented. LHS is a stratified type of

sampling technique wherein the range of uncertain input is divided in N segments which have equal probability, N being the number of samples considered (37). Depending on the types of samples, the relative lengths of each segment can be different based on the specific probability distribution. For example, for uniform distribution all segments are of equal width and for a normal distribution the segments are smaller near the ends of the distribution and larger near the means. For this study 100 samples were chosen and sampled with a normal and uniform distribution. From Table 8 it can be observed that as coefficient B increases, coefficient C reduces. Using the correlation data analysis in Excel and Python, a correlation matrix was generated for these inputs to ensure that the sampling is not independent and there are no unnecessary deviations. The pressure output from CTF was extracted from DAKOTA and the results are summarized in Table 9.

Table 9. DAKOTA output for Uniform Distribution input.

Distribution	**Mean**	**Standard Deviation**	**Lower Confidence Mean**	**Upper confidence Mean**	**Lower Confidence Standard Deviation**	**Upper Confidence Standard Deviation**
Uniform	2.70133	1.8872e-1	2.6638	2.73878	1.6570e-1	2.1923e-1
Normal	2.68286	1.7037e-1	2.6490	2.7166	1.4958e-1	1.9791e-1

CHAPTER 5: CONCLUSIONS, FUTURE WORK AND RECOMMENDATIONS

Based on the simulation conducted, the following conclusions are obtained:

- The friction factor calibration yields a non-linear and not an exact inverse dependence on the Reynolds number as is observed for laminar flows.
- The grid loss coefficient between different methods agrees well with each other. Based on the mesh, smaller the non-dimensional length epsilon, more accurate the planar average will be. It is important to ensure that the mesh immediately upstream and downstream of the spacer grid region is uniform to ensure proper data extraction. The thin-volume averaging is the best as it requires the least amount of post-processing among all three methods.
- Nek5000 is a very computationally expensive software and requires dedicated computing resources for simulations on complex geometries such as mixing vane subchannels.

The goal of this study was to demonstrate the Hi2Lo information method between Nek5000 and CTF. Due to the high computational cost, the simulations have been limited to simplified and shorted length geometries. To form a more complete study the following steps should be carried out:

- For the calibration study, having more data points for calibration would be helpful as that would create a better fit for the B and C coefficients. The Reynolds numbers considered in this study are in the turbulent range, but these are not representative of the nominal operating condition flowrates in a PWR.

- In this study, a very basic uncertainty propagation from Nek5000 to CTF addressing mesh-based uncertainty is demonstrated. This is just one aspect of the uncertain inputs that can affect the solution and hence create uncertainty in CTF outputs. LES turbulence modelling used in this study requires filtering modes, filter ratio and filter weight inputs to model turbulence. A parametric analysis of these inputs would add great insight into the uncertainty propagation in turbulence prediction.
- Nek5000 was originally developed for LES and DNS simulations, but developments have been made to newer version where RANS capabilities have been added and validated. A comparison of the different turbulence models would provide insight into the difference in prediction. Using this, decision can be made for using either of the turbulence models that is computationally less expensive and add the uncertainty if any, to the outputs which can be propagated to CTF.

The CFD code Nek5000 is an exceptional CFD tool with a higher order of accuracy compared to finite volume solvers. The code is highly scalable and has excellent parallelization which means that the computational efficiency is maintained when multiple cores are utilized for this job. However even with this computational efficiency, the computational cost remains significantly high. A few more factors that contribute and are affected by the need of cluster resources are listed below:

- LES Turbulence Modelling: LES turbulence modelling provides insight into the generation of eddies in turbulent flows. However, to extract turbulent parameters, the simulations have to be run long enough to obtain time-averaged parameters. The time-averaging needs to be carried out for at least ten flowthroughs to ensure there are minimal deviation in the time-averaged quantities.

- Reynolds Number: In this study a demonstration of the Hi2Lo of the turbulence modelling is provided which is demonstrated for lower Reynolds numbers. To accurately resolve any given flow, the mesh needs to have a certain level of refinement. This refinement is majorly dependent on the Reynolds number of the flow we need to simulate. Higher the Reynolds number, smaller the mesh elements. This adds to the computational cost in two ways. Smaller the mesh elements are there are higher number of mesh elements required for the domain. This directly increases the degree of freedoms in the mesh. Secondly, smaller the mesh elements, smaller the time-step gets so as to maintain the Courant number condition of <1.0, which increases the wall time to complete one simulation run.
- Nek5000: Being a spectral element code, Nek5000 provides for higher order of accuracy in solutions. But there is also a higher cost of computation associated with this. Other codes that apply Finite Volume Method for CFD problems are known to generate accurate results and are less computationally expensive. Another advantage of such codes is the type of mesh elements allowed for computation. Nek5000 is restricted to hexahedral elements, whereas open-source software packages such as OpenFOAM allow for tetrahedral, prism and pyramid elements.

Priority access to high performance computing resources is essential while using codes like Nek5000. Cluster jobs on Sawtooth cluster at Idaho National Laboratory (INL) are submitted based on the duration of wall time requested. Jobs less six hours are submitted in the 'short' queue and anything over is submitted in the 'general' queue. Requesting jobs with over 1000 nodes for 48 hours sometimes stay in the pending queue for long periods of time.

Relatively jobs for 6 hours are accepted much quicker for the same number of nodes. This work around however, results in the need of constantly monitoring the simulation and resubmitting multiple times a day. A newer version of Nek5000, called NekRS, has the capability of using Graphical Processing Units (GPUs) for calculation of kernels. This has shown significant improvement in the calculation speed-up in comparison of CPUs. An attempt was made to apply the Nek5000 subroutines to NekRS which works but Sawtooth cluster at INL HPC has very limited GPU nodes and hence the simulation ends up in the pending queue for a long time.

REFERENCES

1. Ikeno T. An Application of the Model of Flow Pulsation to the Rod Gap in the Nuclear Fuel Assembly. Flow Modeling and Turbulence Measurements (FMTM2001); 2001.

2. Blyth TS. Development and Implementation of CFD-Informed Models for the Advanced Subchannel Code CTF [dissertation]. ProQuest Dissertations Publishing; 2017.

3. Avramova M. CTF/STAR-CD Off-Line Coupling for Simulation of Crossflow Caused by Mixing Vane Spacers in Rod Bundles. International Conference on Mathematics and Computational Methods Applied to Nuclear Science and Engineering; Rio de Janeiro; 2011.

4. Conner ME, Baglietto E, Elmahdi AM. CFD methodology and validation for single-phase flow in PWR fuel assemblies. Nucl Eng Des. 2010;240(9):2088-95.

5. Gandhir A, Hassan Y. RANS modeling for flow in nuclear fuel bundle in pressurized water reactors (PWR). Nucl Eng Des. 2011; 241(11):4404-8.

6. Bieder U, Falk F, Fauchet G. LES analysis of the flow in a simplified PWR assembly with mixing grid. Prog Nuclear Energy. 2014; 75:15-24.

7. Busco G, Hassan YA. Solution verification of PANS model for a PWR fuel assembly. Nucl. Eng. Des. 2019; 353:110213.

8. Zhang R, Cong T, Su G, Wang J, Qiu S. Investigation on the critical heat flux in typical 5 by 5 rod bundle at conditions prototypical of PWR based on CFD methodology. Appl Therm. Eng. 2020;179:115582.

9. Li Q, Avramova M, Jiao Y, Chen P, Yu J, Pu Z, et al. CFD prediction of critical heat flux in vertical heated tubes with uniform and non-uniform heat flux. Nucl Eng Des. 2018; 326:403-12.

10. Zhang R, Cong T, Tian W, Qiu S, Su G. Prediction of CHF in vertical heated tubes based on CFD methodology. Prog Nuclear Energy. 2015; 78:196-200.

11. Zhang R, Cong T, Su G, Wang J, Qiu S. Investigation on the critical heat flux in typical 5 by 5 rod bundle at conditions prototypical of PWR based on CFD methodology. Appl Therm. Eng. 2020; 179:115582.

12. Xu Y, Brewster RA, Conner ME, Karoutas ZE, Smith III LD. CFD Modeling Development for DNB Prediction of Rod Bundle with Mixing Vanes Under PWR Conditions. Nuclear Technology. 2019; 205(1-2):57-67.

13. Zhang R, Duarte JP, Cong T, Corradini ML. Investigation on the critical heat flux in a 2 by 2 fuel assembly under low flow rate and high pressure with a CFD methodology. Ann Nucl. Energy. 2019; 124:69-79.

14. Pothukuchi H, Kelm S, Patnaik BSV, Prasad BVSSS, Allelein H-. CFD modeling of critical heat flux in flow boiling: Validation and assessment of closure models. Appl Therm Eng. 2019; 150:651-65.

15. Saini N, Bolotnov IA. Detailed Analysis of the Effects of Spacer Grid and Mixing Vanes on Turbulence in a PWR Subchannel Under DFFB Conditions Based on DNS Data. Nucl. Technol. 2021:1-22.

16. Kraus A, Merzari E, Norddine T, Marin O, Benhamadouche S. Direct numerical simulation of fluid flow in a 5x5 square rod bundle. Int J Heat Fluid Flow. 2021; 90:108833.

17. Hu R, Fanning TH. A momentum source model for wire-wrapped rod bundles—Concept, validation, and application. Nuclear Engineering and Design. 2013(262):371-89.

18. Capone L, Benhamadouche S, Hassan YA. Source terms modeling for spacer grids with mixing vanes for CFD simulations in nuclear reactors. Comput Fluids. 2016; 126:141-52.

19. Roelofs F, Uitslag-Doolaard H, Dovizio D, Mikuz B, Shams A, Bertocchi F, et al. Towards validated prediction with RANS CFD of flow and heat transport in a wire-wrap fuel assembly. Nucl Eng Des. 2019; 353:110273.

20. Fang J, Shaver DR, Tomboulides A, Min M, Fischer P, Lan Y, et al. Feasibility of full-core pin resolved CFD simulations of small modular reactor with momentum sources. Nucl. Eng. Des. 2021; 378(C):111143.

21. Rowe DS, Angle CW. Crossflow Mixing between Parallel Flow Channel during Boiling Part III: Effect of Spacers on Mixing between Two Channels. BNWL-371 (Part III).

22. Rowe DS, Johnson BM, Knudsen JG. Implications concerning rod bundle crossflow mixing based on measurements of turbulent flow structure. Int J Heat Mass Transfer. 1974;17(3):407-19.

23. Rehme K. The structure of turbulence in rod bundles and the implications on natural mixing between the subchannels. Int J Heat Mass Transfer. 1992; 35(2):567-81.

24. Yao SC, Hochreiter LE, Leech WJ. Heat-Transfer Augmentation in Rod Bundles Near Grid Spacers. ASME. J. Heat Transfer. 1982 February; 104(1):76–81.

25. McClusky HL, Holloway MV, Beasley DE, Conner ME. Development of Swirling Flow in a Rod Bundle Subchannel. ASME. J. Fluids Eng. 2002 September; 124(3):747-55.

26. Fen Shen Y, Dong Cao Z, Gang Lu Q. An investigation of crossflow mixing effect caused by grid spacer with mixing blades in a rod bundle. Nucl. Eng. Des. 1991;125(2):111-9.

27. Jeong H. Evaluation of Turbulent Mixing between Sub-Channels with a CFD Code. Sixth International Conference on Nuclear Thermal Hydraulics, Operation and Safety (NUTHOS-6), Nara, Japan; 2004.

28. Salko RK, Pointer WD, Delchini M, Gurecky WL, Clarno KT, Salttery SR, et al. Implementation of a Spacer Grid Rod Thermal-Hydraulic Reconstruction (ROTHCON) Capability into the Thermal-Hydraulic Subchannel Code CTF. Nucl. Technol. 2019; 205(12):1697-706.

29. Gilkey LN, Sandia National Lab. (SNL-NM), Albuquerque,NM (United States). CASL Thermal Hydraulic Hi2Lo Applications. United States; 2020.

30. Kulkarni NA, Holler D, Avramova M, Delchini MG. INVESTIGATION OF DIFFERENT PLANE-AVERAGING TECHNIQUES IN NEK5000 FOR HIGH-TO-LOW INFORMATION OF CTF. Manuscript submitted for publication.

31. Deville MO, Fischer PF, Mund EH. High-Order Methods for Incompressible Fluid Flow. Cambridge: Cambridge University Press; 2002.

32. Pope SB. Turbulent Flows. Cambridge University Press; 2000.

33. Stolz S, Schlatter P, Kleiser L. High-pass filtered eddy-viscosity models for large-eddy simulations of transitional and turbulent flow. Physics of Fluids. 2005; 17(065103).

34. Dillon Shaver-ANL/usrcode [Internet]. Available from:https://github.com/dshaver-ANL/usrcode/blob/master/utilities.f.

35. Childs H, Brugger E, Whitlock B, Meredith J, Ahern S, Pugmire D, et al. VisIt: An End-User Tool For Visualizing and Analyzing Very Large Data. High Performance Visualization--Enabling Extreme-Scale Scientific Insight. 2012:357-72.

36. Avramova MN, Salko RK. CTF Theory Manual. CASL-U-2016-1110-000 ed. Oak Ridge, TN: Oak Ridge National Laboratory; 2016.

37. Adams BM, Ebeida MS, Eldred MS, Jakeman JD, Swiler LP, Stephens JA, et al. Dakota, a multilevel parallel object-oriented framework for design optimization, parameter estimation, uncertainty quantification, and sensitivity analysis. 2014.

38. Rubin A, Schoedel A, Avramova M, Utsono H, Bajorek S, Velasquez-Lozada A. OECD/NRC Benchmark based on NUPEC PWR subchannel and bundle tests (PSBT): Volume I Experimental Database and Final Problem Specifications NEA/NSC/Doc. 2010.

39. Coreform Cubit (Version 2020.2) Coreform LLC [Internet]. []. Available from: http://coreform.com.

40. Holler D, Kulkarni NA, Avramova MN. Computational Fluid Dynamics Mesh Generation of the PSBT Benchmark Subchannels for Use with Nek5000. Mathematics & Computation (M&C) 2021; October 2021.

41. Coreform Cubit: Metrics for Hexahedral Elements [Internet]. Available from: https://coreform.com/cubit_help/mesh_generation/mesh_quality_assessment/hexahedral_metrics.htm.